SHARP Storage - Project no 327342

Updated catalog and focal mechanism database

Deliverable 2.4

Organisation(s)	Delft University of Technology, NORSAR, GEUS, University of Oxford, BGS, Shell and BP
Author(s)	E. Martuganova , T. Kettlety , A. Jerkins, D. Kühn, N. Langet, J. Schweitzer, B. Baptie, T. Dahl-Jensen, J. Asplet, P. Voss, J. M. Kendall, A. Barnhoorn
Reviewer(s)	Tine Larsen (GEUS) & Cornelis Weemstra (KNMI)
Type of deliverable	Database & Report
WP	2
Issue Date	May 2024
Document version	1

Contents

Acknowledgements

We would like to thank all the partners of the project involved in the data collection for the North Sea seismological bulletin, as well as for the seismic waveforms. The authors would like to sincerely acknowledge the Geological Survey of Denmark and Greenland (GEUS), the Royal Netherlands Meteorological Institute (KNMI), the British Geological Survey (BGS), NORSAR, British Petroleum (BP), Equinor, The Indian Institute of Technology Bombay (IIT Bombay), INEOS, Norwegian Geotechnical Institute (NGI), Norwegian University of Science and Technology (NTNU), University of Oxford, Risktec, Rockfield, Shell, TU Delft, Wintershall Dea.

This study was possible based on data collected and provided to the public from the following seismological networks: German Regional Seismic Network (GR, Federal Institute for Geosciences and Natural Resources, 1976), Danish Seismological Network (DK, Seismisk Tjeneste, 2023), GEOFON Seismic Network (GE, German Research Centre for Geosciences GFZ, 1993), Netherlands Seismic and Acoustic Network (NL, Royal Netherlands Meteorological Institute (KNMI), 1993), NORSAR Station Network (NO, NORSAR, 1971), University of Bergen Seismic Network (NS, University of Bergen, 1982), the Magnus temporal network (2006-2008) (Z6, (Weidle et al., 2010), the Belgian Seismic Network (BE, Royal Observatory of Belgium, 1985), the Great Britain Seismograph Network (GB, British Geological Survey, 1970) as well as the Kiel University Earthquake Monitoring (KQ, Christian Albrechts - Universitat zu Kiel, 2017).

We also would like to sincerely thank Sebastian Heimann (University of Potsdam, Germany) for his flexibility in adapting the Squirrel algorithm to this specific task and helping with its application, as well as for his advice on using the Pyrocko Python package and Grond software for moment tensor computations.

This report is part of the SHARP Storage research program ('Stress History and reservoir pressure for improved quantification of CO2 storage containment risks') funded through ACT3– Accelerating CCS Technologies (Project No ACT320011), by RCN and Gassnova (Norway), ROV (The Netherlands), DST (India), BEIS (UK) and EUDP (Denmark).

Executive summary

This report describes updates to the North Sea seismicity event bulletin in which all earthquakes from databases of the countries bordering the North Sea are amalgamated into a single bulletin. This is the first dataset of its kind and makes up the most complete and homogeneous bulletin for the North Sea at the time. A comprehensive evaluation of the natural earthquake activity provides important information on the stress field and faulting mechanisms near the proposed reservoirs for carbon capture sequestration. The collected information is crucial for the understanding of the response of the reservoir and caprock to large-scale fluid injection. This deliverable describes the subsequent analysis comprised of event magnitudes, locations, and moment tensor inversion to derive source mechanisms.

SHARP's North Sea earthquake bulletin is updated from the earlier produced bulletin presented in deliverable D2.1. The new bulletin comprises mostly the removal of explosion events and minor formatting issues and constitutes the most complete and - despite unresolved challenges - the most homogeneous representation of North Sea seismicity available to date. Two byproducts of the new bulletin are a catalogue consisting of prime information and a catalogue extended to a larger region as base for the seismic hazard analysis performed in WP 5. Furthermore, analyses are performed on different magnitude scales. The usage of different formulas and input data makes direct comparisons between magnitudes difficult, especially for the local magnitudes. An analysis is also performed to relocate events within the North Sea bulletin, making use of the abundance of the new compilation of phase information. Our effort now also includes collecting waveforms for events that occurred later than 1990 and had magnitudes larger than M 3.5, although quality control of these waveforms was not possible yet. Lastly, previously computed focal mechanisms are collected, and new moment tensors are calculated mainly for the larger magnitude events. We conclude that for many events, the number of available records as well as the data quality is not sufficient for reliable estimates of, e.g., source mechanisms.

Therefore, our main recommendation is to install more offshore seismic stations, particularly to add stations close to potential sources to increase the number of near-source observations and fill the azimuthal gaps in the station's coverage to enable a more precise event location, event depth estimates and source mechanism analysis as well as enhance magnitude estimates. Especially with a view on the start up of CO_2 injection and storage, it is important to establish a more reliable event analysis specifically for lower magnitude events that may potentially be induced events during operations. Without a dedicated plan to install a larger number of stations within the North Sea, a stable event analysis and derivation of estimates of stress orientations remain only possible for the largest magnitude event, not to mention the impossibility of a discrimination of natural and induced seismicity.

1 Earthquake bulletin

Work has continued in improving the quality of the data collected in the bulletin and catalogues detailed in SHARP deliverable D2.1. We detail these improvements and alterations here.

1.1 Current status

The earthquake bulletin for the North Sea was the first deliverable from WP2 of SHARP. This was the first dataset of its kind, and made up the most complete and homogeneous bulletin for the North Sea at the time. This dataset has enabled a number of the tasks in this and other work packages.

The event bulletin produced by WP2 task 2.1 has been altered slightly since its publication in Q4 2022. Details of the original dataset can be found in SHARP Deliverable D2.1. Further work on this dataset has mostly comprised of the identification and isolation of explosions (described in section 1.2) as well as the removal of minor formatting errors. These minor errors were found during subsequent analysis, and were a product of errors in the ISF-writing scripts. Two minor updates of the bulletin (1.1 and 1.2) were uploaded to the project's data sharing site since the publication of the first deliverable.

Figures 1 and 2 show the equivalent figures for the current version of the bulletin data as published in D2.1 (Figure 4.5, Deliverable D2.1).

Our combined bulletin is more complete than any of the individual catalogues from each of the national seismological agencies bordering the North Sea as well as the internationally available catalogues of ISC and GEOFON, from which the data originated. This is shown in Figure 3. The national catalogues naturally report more events which are geographically closer to their networks. Thus, by combining data we clearly can improve the understanding of events in the North Sea region as a whole.

1.2 Explosion removal

The identification and isolation of explosions constituted the next step after the delivery of D2.1. In this context, we defined an explosion as any seismically detected event that is not the result of shear failure of rock in the subsurface (i.e., an earthquake). This could be the result of an actual explosion (e.g., deliberate military or industrial detonations), or some other event that generates an impulsive source of acoustic energy measurable over long distances. An example of the latter includes the collapse of the oil rig Piper Alpha on July 6^{th}-7^{th} 1988.

Different approaches were tested, including clustering the events based on their location inside the exclusive economic zone of the bordering North Sea countries and corresponding reporting agencies. Due to contradictions in data provided by different data centres, it was decided only to exclude events from the catalogue if all reporting agencies marked this catalogue entry as "sm" (suspected mine explosion), "kh" (known chemical explosion), "sh" (suspected chemical explosion), "kx" (known experimental explosion), "sx" (suspected experimental explosion), "kn" (known nuclear explosion) or "sn" (suspected nuclear explosion). This way, we prevented the potential loss of the earthquake's entries due to disagreements between multiple interpretations of the event type.

In total, 5,048 events were identified as likely or potential explosions (a map of which is shown in Figure 4). The distribution of the events varies both spatially and temporally. Most of the selected

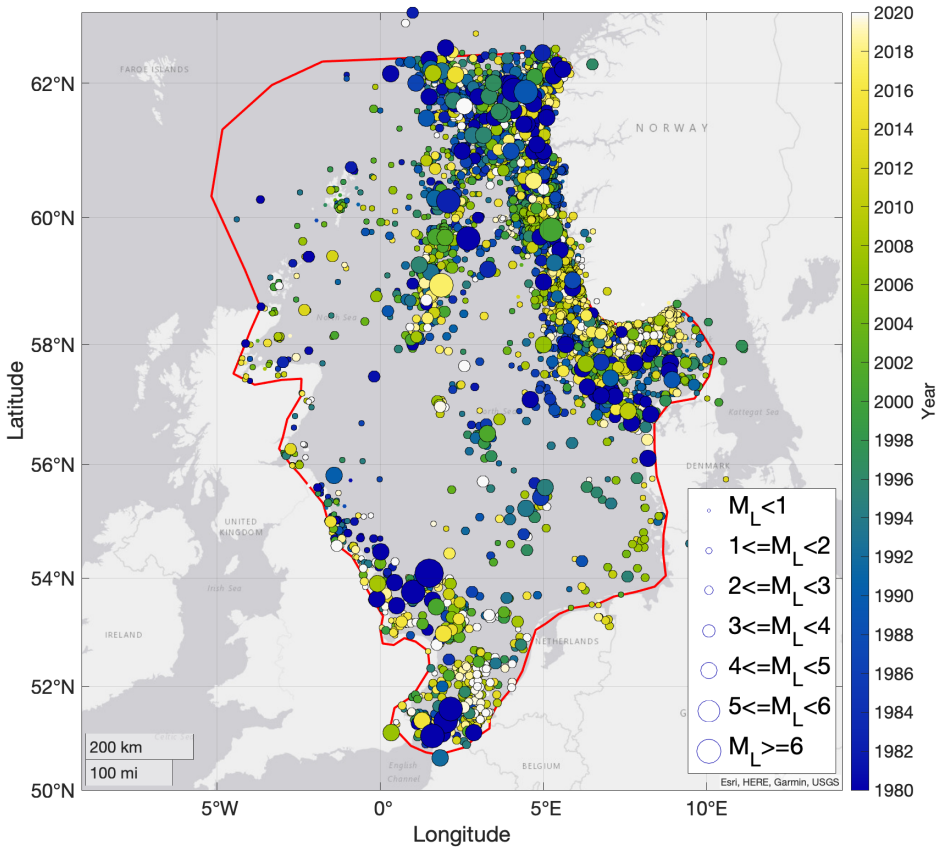

FIGURE 1: Map of the epicentral locations for prime event entries in the current bulletin. 15,231 events are shown, 5,048 of which have been identified as likely or suspected explosions (see section 1.2). The red line shows the outline of the polygon used to discriminate events of interest (i.e., those within or close to the North Sea). Events are shown as circles, coloured by time (in this plot limited from 1980 to 2020) and sized by magnitude.

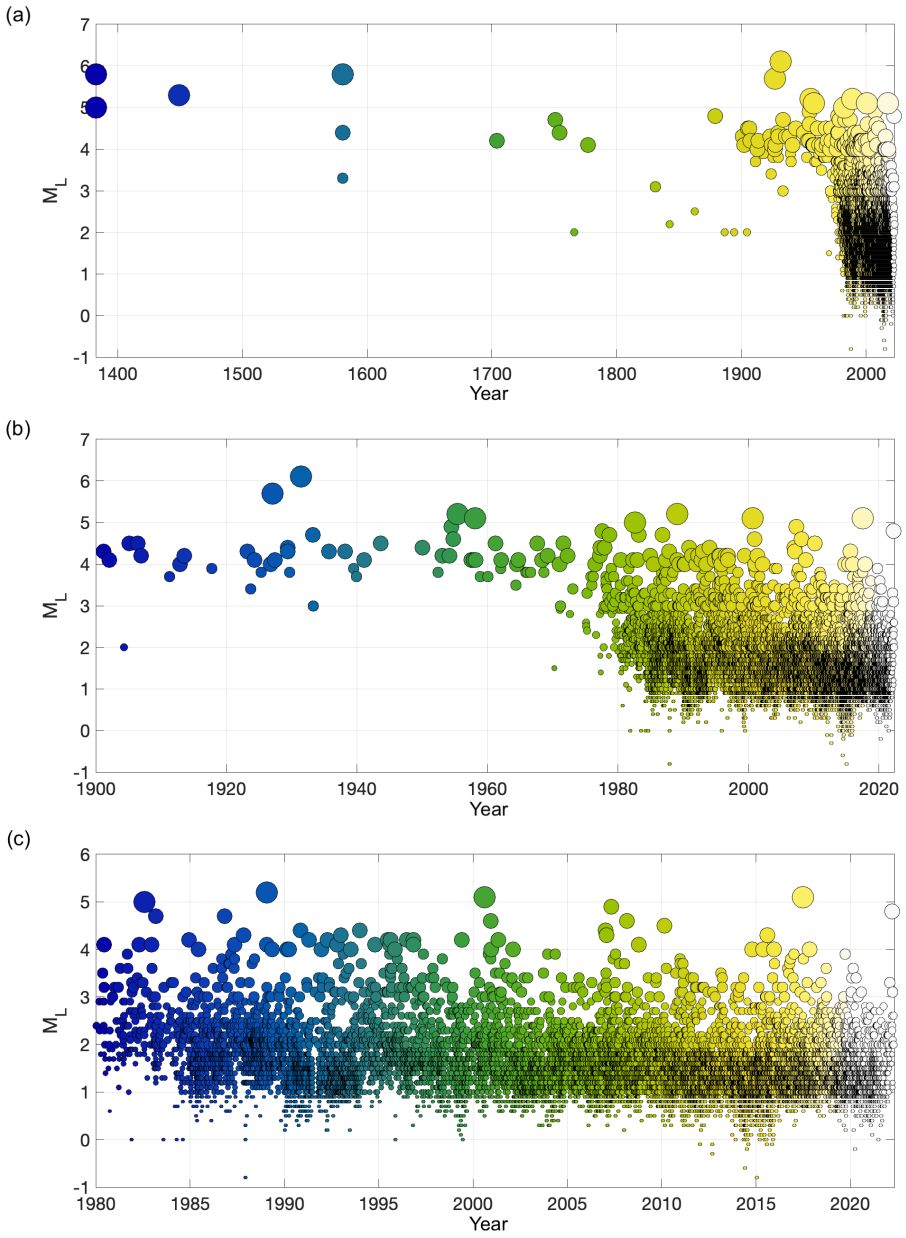

FIGURE 2: Magnitude-time distribution of all events in the bulletin, symbol formatting as in Figure 1. Three time windows are shown: (a) the complete bulletin, starting from the earliest event (May 1382); (b) events from 1900, when instrumental records of events became more common in Europe; and (c) events from 1980, when detection and location of events improved significantly as national seismic networks matured. Local magnitude M_L is employed.

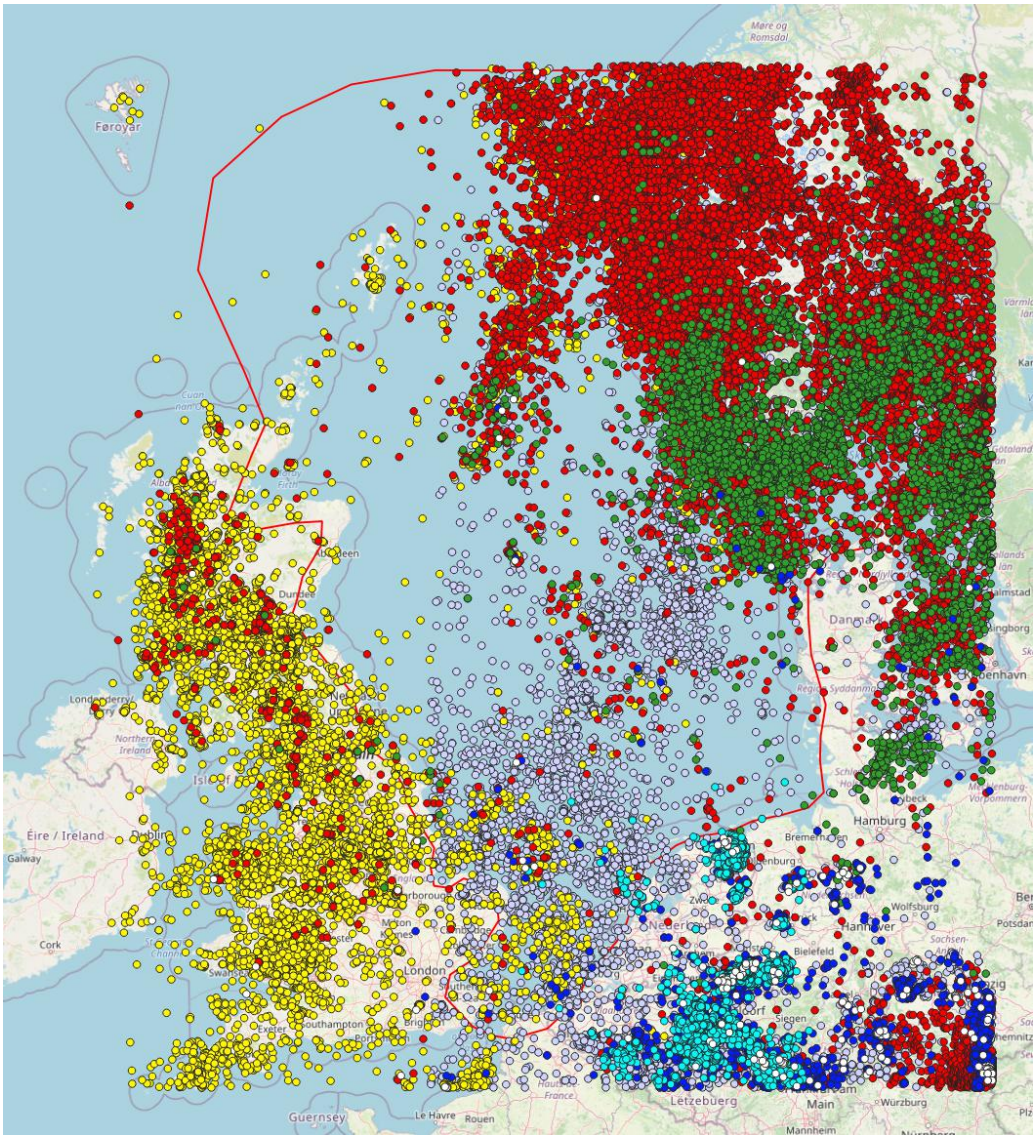

FIGURE 3: Comparison of catalogues of seismological agencies bordering the North Sea: turquoise: Netherlands, dark blue: Germany, yellow: UK, green: Denmark, red: Norway, white: GEOFON, grey: ISC

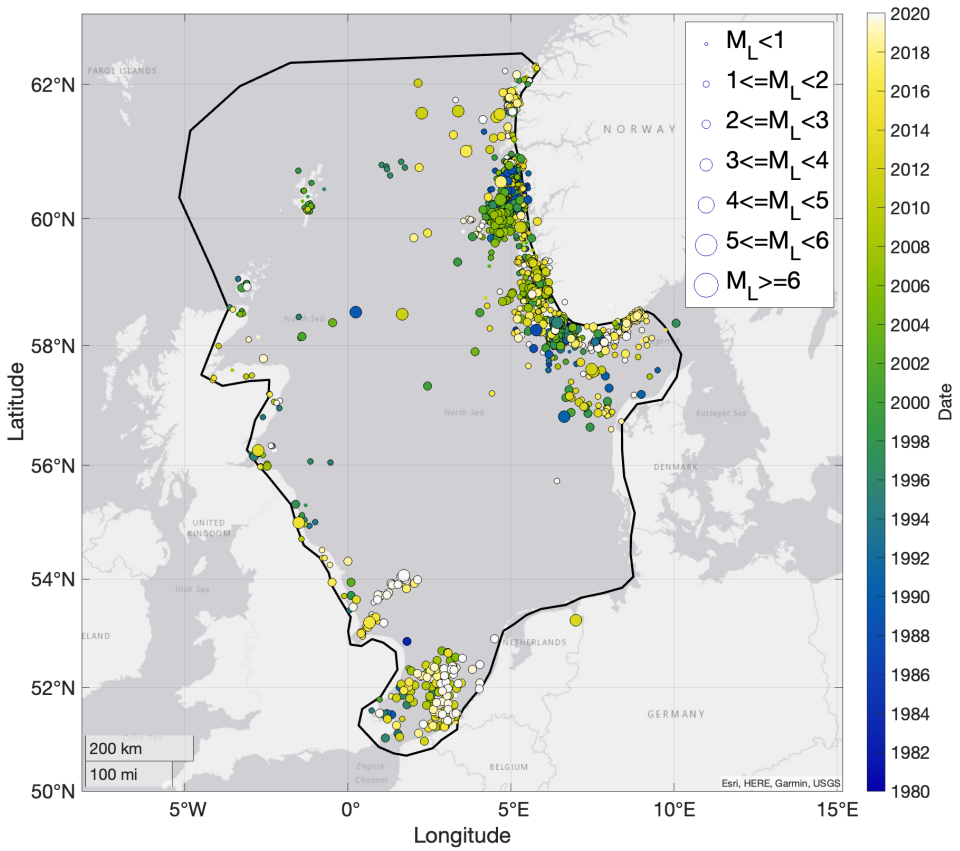

FIGURE 4: Map of epicentral locations of 5,048 likely explosions. Symbol formatting as in Figure 1.

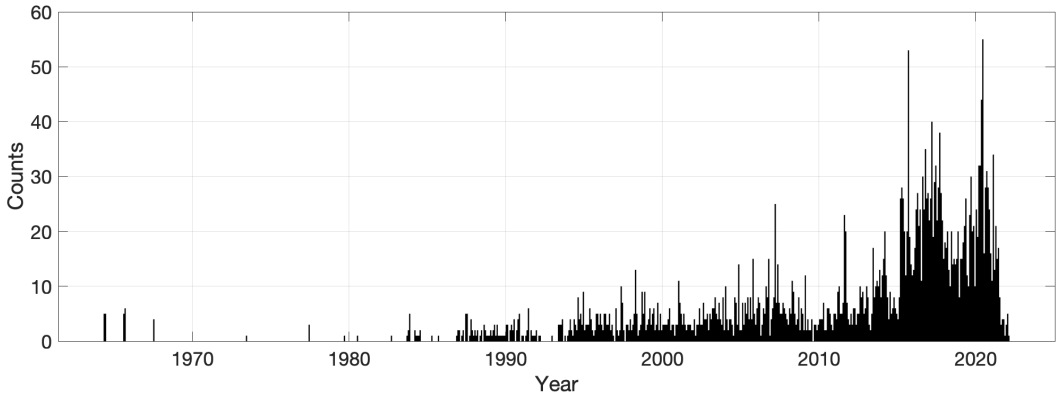

FIGURE 5: Histogram of likely explosions through time, with monthly bins.

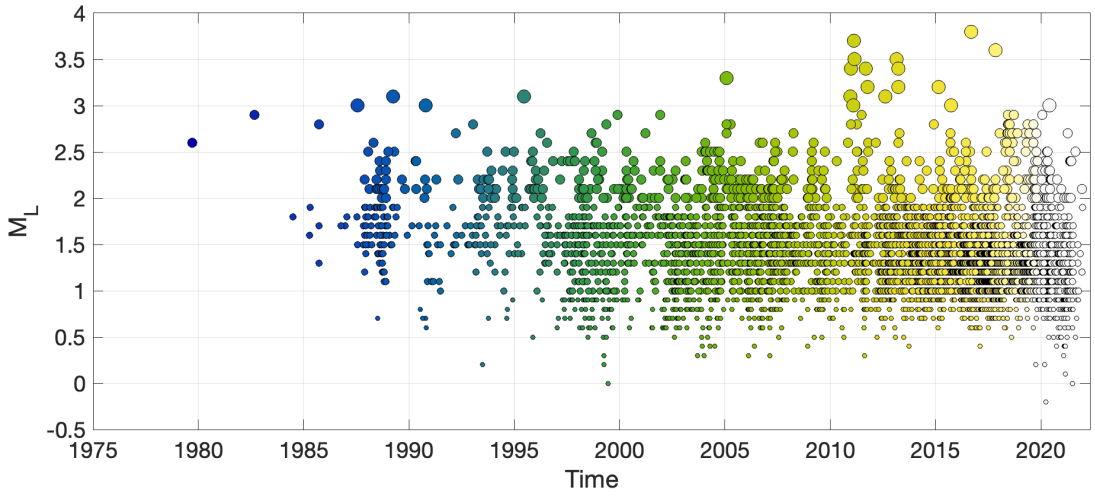

FIGURE 6: Local magnitude against time of the likely explosions.

explosion events are located near coastal areas, with some exceptions, typically associated with oil and gas exploration activities. In terms of temporal distribution, the number of reported explosions consistently increased starting from 1990 (Figure 5).

Most likely, this is an expression of an enhanced coverage by seismic instruments, resulting in a lower magnitude of completeness for the North Sea, rather than an increase in military or industrial operations. The majority of suspected explosion entries have low magnitudes $M_L \leq 2$ (Figure 6), although a few exceed a M_L of 3.5.

A considerable amount of selected entries do not possess magnitude estimates, especially before 1980. The statistical analysis of these entries shows that most of the explosions occur during the workdays from Monday to Friday (Figure 7a). In terms of distribution throughout the time of the day, most of the detonation work is conducted in the afternoon, following operations in the morning, with only minor exceptions at night (Figure 7b).

1.3 Event magnitudes

Event sizes, or magnitudes, are a key parameter in the characterisation of earthquakes. Magnitudes are an important input into many different types of seismological, geomechanical, and hazard analy-

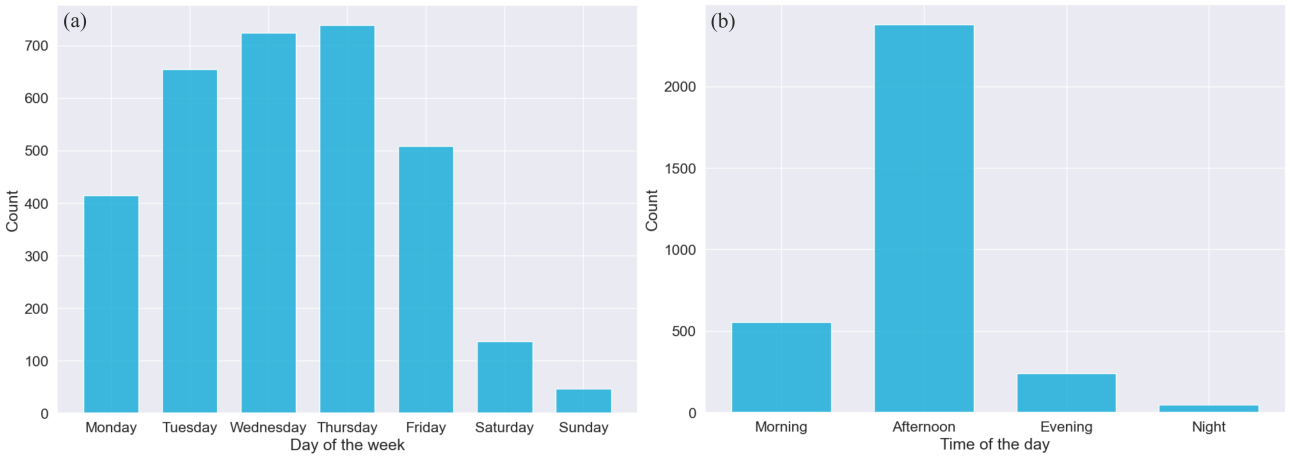

FIGURE 7: Histogram of events marked as explosions grouped by (a) day of the week and (b) time of the day.

sis. They are also often the sole parameter quoted in news media and by the public when referring to specific events. These underscores the importance of accurate estimation of earthquake magnitudes and their associated uncertainties.

Magnitudes can be computed in different ways, using different input data and methodologies. For a more detailed explanation of different magnitude types, the reader is directed to Stork et al., 2014; Shearer, 2019 and Luckett et al., 2019.

In the current version of the catalogue, many magnitudes are reported, both in terms of the number of records and magnitude type. Figure 8 shows that there are over 20 different types listed, from over 43,000 magnitude records. These come from several dozen listed sources. This wide variety of data types and sources makes systematic analyses of the data challenging. This is mainly due to the variety of processing and reporting methods used to produce the magnitude and the underlying amplitude data, both of which are collected in the bulletin.

The variation in data type is particularly acute for local magnitude M_L. This magnitude scale uses the amplitude recorded by a seismometer, after a filter is applied to the signal that simulates the response that would be recorded by a older type of instrument called a Wood-Anderson seismometer. However, many different M_L scales are used in the North Sea region, and different input data are used for these magnitudes estimate. For example, the way in which the amplitudes of either P- or S-wave phases are computed differs between neighbouring agencies. One may use peak to peak amplitude on the vertical component, whilst another may use the zero-to-peak ampitude on the horizontals.

However, in the bulletin these would all be simply reported as "M_L". A review of the reported local magnitude scales shows that more than 6 different scales are reported in the North Sea region, some using the amplitude recorded on the horizontal components of the seismometer, some the vertical, some both. Some use the zero-to-peak amplitude, some the peak-to-peak divided by 2, some the arithmetic mean of the horizontals. This variation in methodology leads to incompatibility of many of the magnitudes in the bulletin, with further homogenisation required in order for robust comparisons to be made.

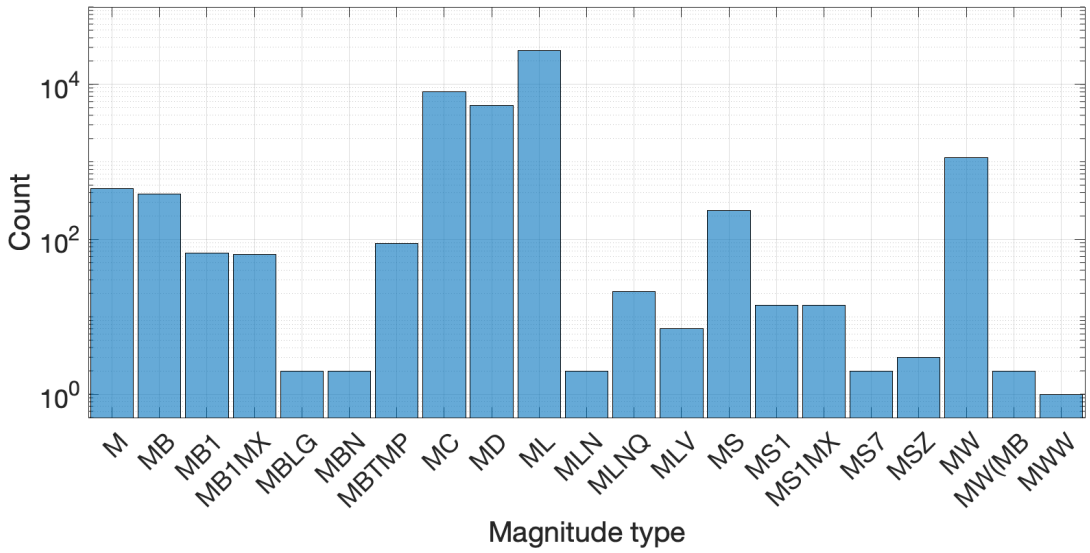

FIGURE 8: Histogram of the types of magnitude which are reported in the current bulletin. Many are variations of commonly computed types, like local magnitude M_L, or moment magnitude M_W.

The differences in the formulae used to calculate local magnitudes is further exacerbated by the attenuation properties of the North Sea region. The North Sea is known to dampen Lg waves significantly (Gregersen and Vaccari, 1993), which results in systematic variations in the amplitude of earthquake arrivals used to measure magnitude. With different scales and these effect, this leads to - sometimes significant - variations in the magnitudes that are reported and discussed for earthquakes in the North Sea. An example of this is shown in Figure 9 listing the magnitudes reported for the 21^{1st} March 2022 earthquake with M∼5 that took place in the northern North Sea. These vary by 0.8 magnitude units resulting from the variation in scales and input data as well as station-to-station variations in amplitudes induced by attenuation or near surface effects. The resulting differences in magnitude introduce a communication challenge, potentially confusing the public, and could also lead to regulatory uncertainty if magnitudes are to be used in some kind of monitoring framework for mitigation of induced seismicity.

Investigating these complicating factors, and the lack of uncertainty information in the collected magnitudes, will be the focus of an additional study in the time remaining in the SHARP project. This is planned to be delivered in an academic publication. The initial focus of this study will be on systematically measuring amplitudes using the waveform data currently collected, to quantify the station variability in local and body wave magnitude, and the effect of attenuating structures in the North Sea. This forms the base of a later development of a unified local magnitude scale applicable to the North Sea.

Figures 10 and 11 show the amplitude distance relationships for the data that currently exists in the bulletin together with the magnitude scales of both the British Geological Survey (BGS) and the Norwegian National Seismic Network (NNSN). Whilst amplitude data exists from a wide range of distances (the farthest coming from teleseismic recordings), the most relevant data for this study is collected

Event 11980 North Sea

Date	Time	Err	RMS	Latitude	Longitude
2022/03/21	05:32:53.00			61.6700	2.5800
2022/03/21	05:32:53.41	0.30	0.80	61.6180	2.1299
2022/03/21	05:32:53.49	1.00	0.50	61.5527	2.3926
2022/03/21	05:32:54.00			61.4400	2.3900
2022/03/21	05:32:55.10	0.80	0.60	61.5430	2.2680
2022/03/21	05:32:55.30	0.00	0.60	61.5580	2.3870
2022/03/21	05:32:55.60	0.10	0.90	61.6200	2.1200
2022/03/21	05:32:55.80		1.30	61.7050	2.5420
2022/03/21	05:32:55.90	3.30	1.50	61.6030	2.3270
2022/03/21	05:32:55.93	0.60	0.80	61.4410	2.2840
2022/03/21	05:32:56.47			61.5300	2.5700
2022/03/21	05:32:57.50	0.10		61.6700	2.2100
2022/03/21	05:33:02.51			60.8079	1.8213
2022/03/21	05:32:55.34	0.00	0.56	61.5584	2.3871

(#PRIME)

Magnitude		Err	Nsta	Author	OrigID
mb	5.4		702	NEIC	7650B
Mww	5.2		43	NEIC	7650B
mb	4.8		35	IDC	6E16B
mbtmp	4.9		46	IDC	6E16B
ML	4.8		11	IDC	6E16B
MS	4.8		69	IDC	6E16B
MB	5.5			MOS	70539
ML	5.2			BGS	637A0
ML	4.7			NAO	697BE
mb	5.2		46	AUST	718B7
Mw	5.3		21	AUST	718B7
ML	4.8			DNK	629E7
Ms	4.6			DNK	629E7
MS	4.9			DNK	629E7
ML	4.6			BER	63955
MW	4.7			BER	63955
ML	5.4			BGR	6E46B
MW	5.2			GFZ	6EA11
MW	5.3		129	GCMT	6BE8E
mb	4.9		10	SFS	6216C
ML	5.1		10	SFS	6216C
ML	4.7			NORSAR	B3B9D

FIGURE 9: A screenshot of the origin and magnitude blocks for the 21[1st] March 2022 earthquake with M∼5.

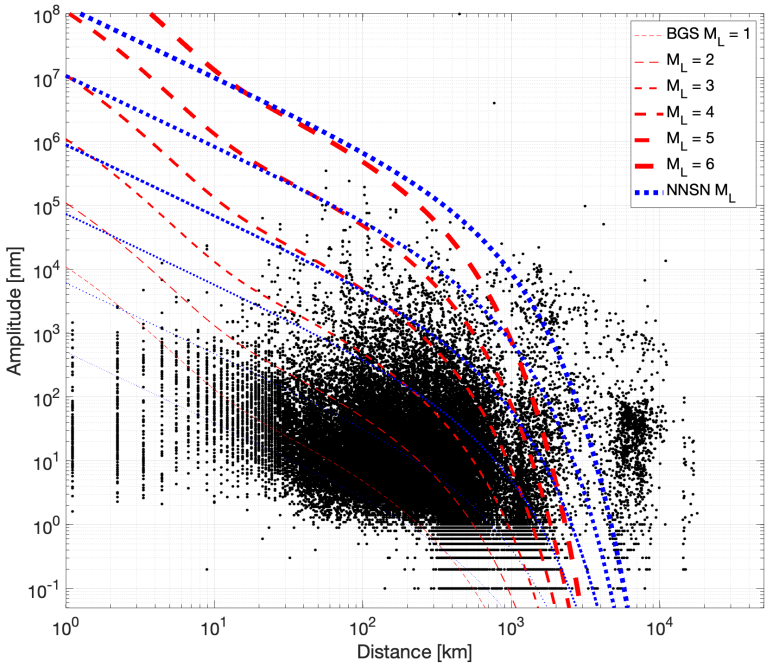

FIGURE 10: Amplitude-distance measures as recorded in the current bulletin, as shown by the black dots. Red dashed and blue dotted lines show the local magnitude M_L scales for the British Geological Survey (BGS) and Norwegian National Seismic Network (NNSN), respectively. Thickness of lines represents the amplitude value for scales at different magnitude levels, with M_L 1 being the thinnest, and M_L 6 being the thickest.

at distances less than 1,000 km (i.e., European data) highlighted in Figure 11. The magnitude scales shown here clearly deviate by over ∼0.5 magnitude units from around 400 km distance, showing again the differences in reported magnitudes for the same events recorded on either side of the North Sea. Figure 12 displays event-station distances for the amplitudes recorded in the bulletin. There are clearly far more recordings in the near field (<200 km) with a secondary peak at around 400 km. The dearth between both peaks illuminates the lack of stations in the near field, with events of a certain size being recorded by stations from across the North Sea (above ∼400 km).

The relationship between local magnitude M_L and moment magnitude M_w is important for seismic hazard analysis as it can be used to estimate magnitude information if only M_L measurements are available, mostly for historic events (Dost et al., 2018, e.g.,). Figure 13 shows the M_w-M_L relationship when the median M_L and M_w are taken for all of the events in the catalogue. Far fewer events have a reported M_w, as it is commonly only computed for the larger (M>3) earthquakes. The characteristic divergence between M_L and M_w at lower (M<3) magnitudes is observed.

However, due to the complicating factors discussed above, it is not strictly robust to compare the average M_L and M_w values across the whole catalogue, as they have been computed using different methods and input data. Figure 14 shows the M_w-M_L relationship when just the magnitudes reported by a single source are compared, in this case the University of Bergen.

The fitted relationship is different from that shown in Figure 13, but not wildly so. Other tasks within

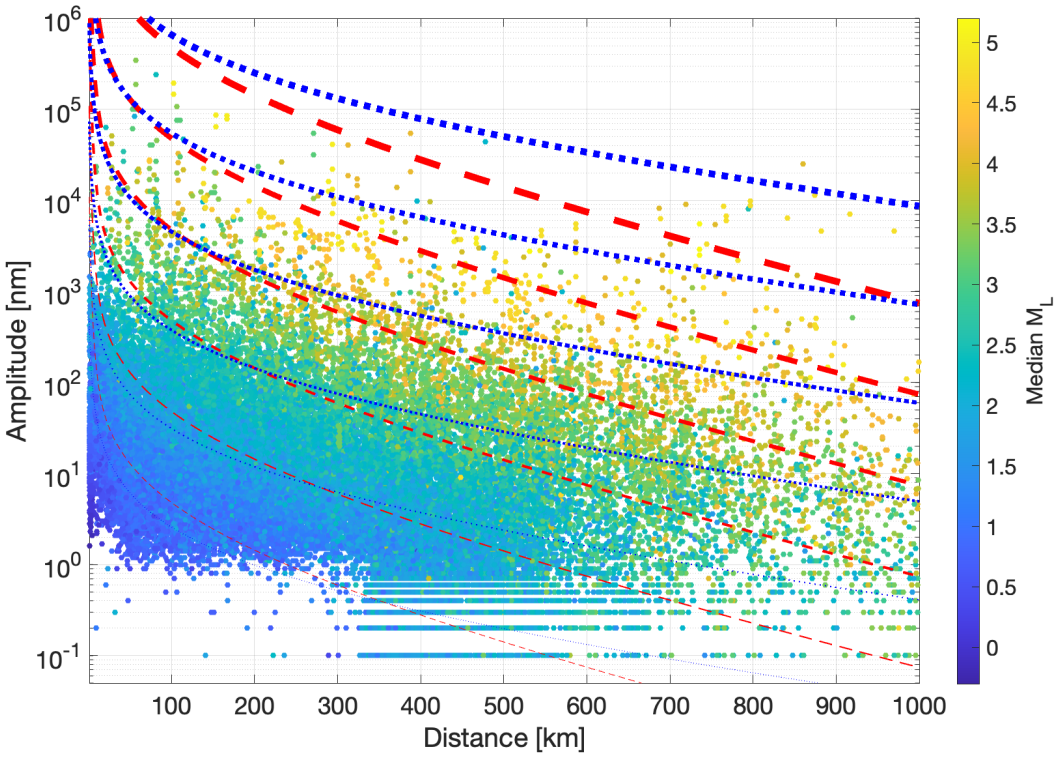

FIGURE 11: Amplitude-distance as recorded in the current bulletin, coloured by the median M_L for that event. The BGS and NNSN magnitude scales are shown as in Figure 10.

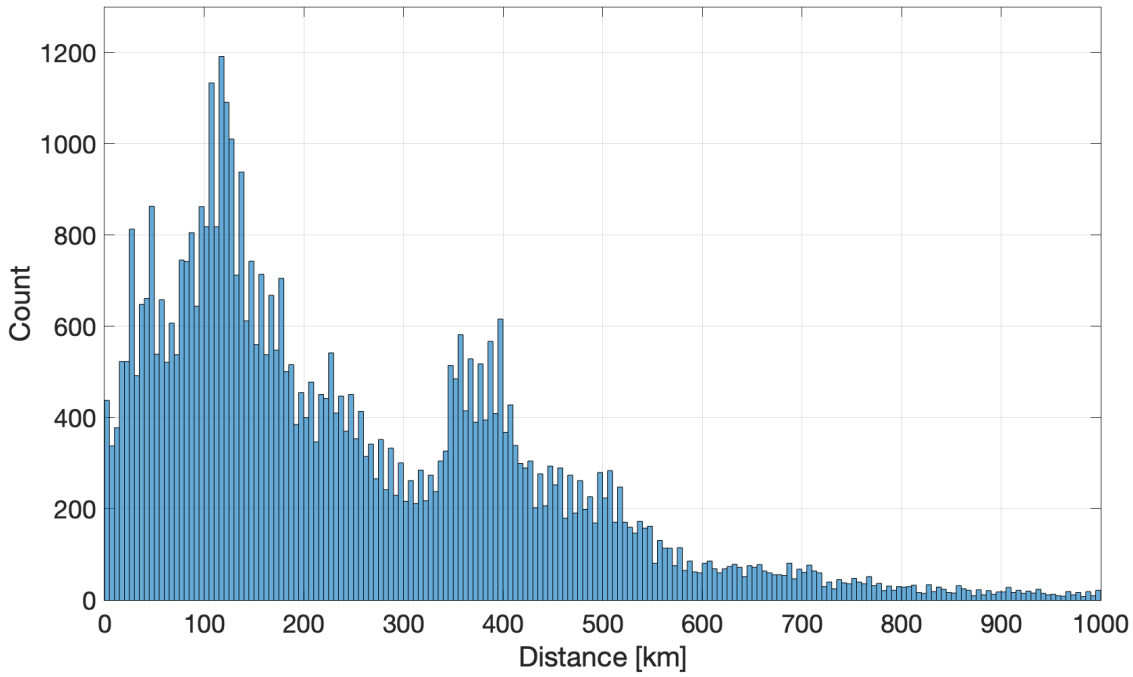

FIGURE 12: Histogram of station distances at which amplitude data is recorded in the current bulletin.

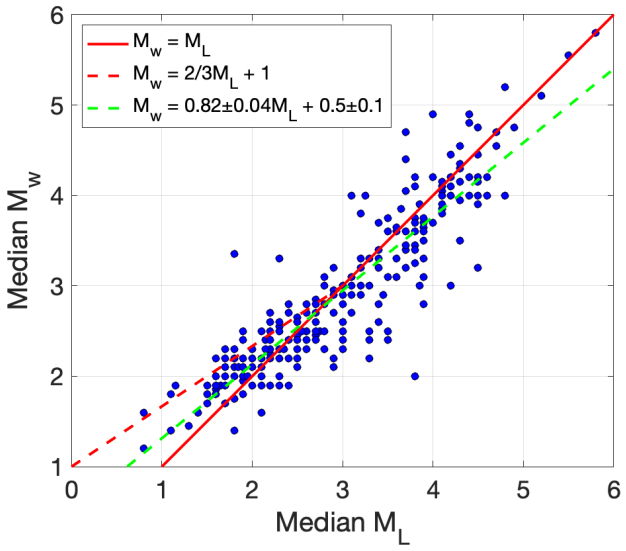

FIGURE 13: Blue points show the median local and moment magnitudes (M_L and M_w, respectively) for each event in the bulletin. Only the subset events with reported M_w values are shown. The red solid line shows the line of unity (M_w=M_L). The red dashed line shows the theoretical deviation between M_w and M_L that is expected at low (M∼3) magnitudes due to attenuation effects. The green dashed line shows the fitted M_w-M_L relationship based on the data. The equation for this fitted line is shown in the legend.

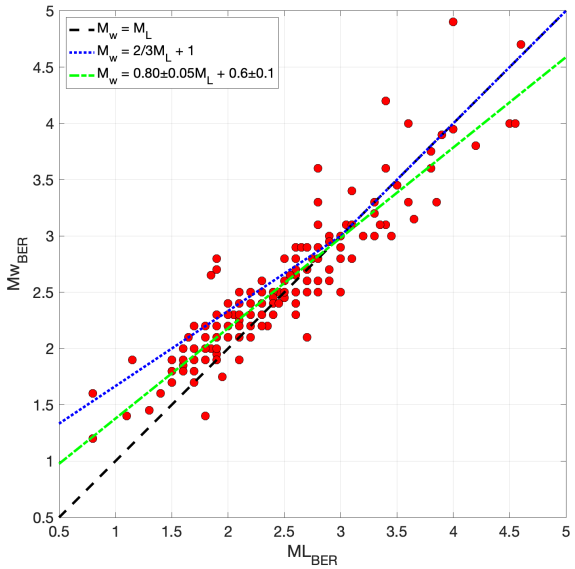

FIGURE 14: Red points show the local and moment magnitudes (M_L and M_w, respectively) reported by the University of Bergen (BER). Only events for which BER was the source of the M_L and M_w are shown.The black dashed line shows the line of unity (M_w=M_L). The blue dotted line shows the theoretical deviation between M_w and M_L that is expected at low ($M\sim 3$) magnitudes due to attenuation effects. The green dashed line shows the fitted M_w-M_L relationship based on the data. The equation for this fit is shown inset.

this work package are producing moment magnitudes. The stress drop measurement in Task 2.3 analyses the event spectra, and thus get moment magnitude estimates. The moment tensor inversion for source mechanism in Task 2.1 also produces an estimate of M_w. Along with the planned reanalysis of the event local magnitudes, a revised M_w-M_L will likely be possible.

1.4 Seismic hazard catalogue

For seismic hazard analysis, felt earthquake occurrence rates need to be quantified both within and outside the region of interest. The current version of the North Sea earthquake catalogue was formed using a spatial filter, referred to as the North Sea polygon (see Deliverable 2.1 for details). For the seismic hazard analysis that is being conducted in Task 5.2 of SHARP, the current bulletin needed to be expanded, including event data for a 300 km area around the polygon. This larger region is shown in Figure 15.

Figure 15 also displays the events that have now been added to this supplemental version of the bulletin and prime catalogue. The event data was collected from the European Seismic Hazard Model 2020 (ESHM20), which contains event times, hypocentres, and moment magnitudes. Data for 579 events were added to this expanded version of the bulletin from the ESHM20 database. 122 of these events were within the original polygon, and 457 were outside.

Where there was already data in the bulletin for a ESHM20 event (i.e., for the 122 events noted above), the origin and magnitudes were folded into the appropriate data blocks. This merging of event data was manually quality-controlled to ensure no false mergers occurred. Earthquakes outside the polygon were added as wholly new events. The ESHM20 origins were listed with the event type “ke”, as they are clearly known earthquakes, quality-controlled by the ESHM20 consortium. These supplementary events will also not be relocated.

It may appear that there are a great number of larger magnitude events in the supplemental region shown in Figure 15. This is an effect of selection, completeness, and plotting. The ESHM catalogue provides data for larger events, dating back as far as possible. These larger events naturally only have magnitudes which are relevant to seismic hazard (generally $M>3$). Equivalently large and historic events that may have occurred in the middle of the North Sea study region likely were undetected, and thus not present in the historical data which makes up most of the ESHM catalogue.

The use of this catalogue for seismic hazard analysis will be detailed in the SHARP WP5 deliverable 5.5.

1.5 Prime catalogue

When an event catalogue is produced from the North Sea bulletin, a single origin, location, and set of magnitudes must be selected for each event – this event data is known as the “prime” origin. Prior to this deliverable, the catalogue’s primes were selected based on the primes reported by the individual agencies. That is, the first row of the origin block was selected as the prime, as this was likely considered the prime by the underlying agency.

This is clearly not utilising the benefits of the newly integrated data in the bulletin, and thus, a new method for prime catalogue preparation is now employed on an event-by-event basis as follows:

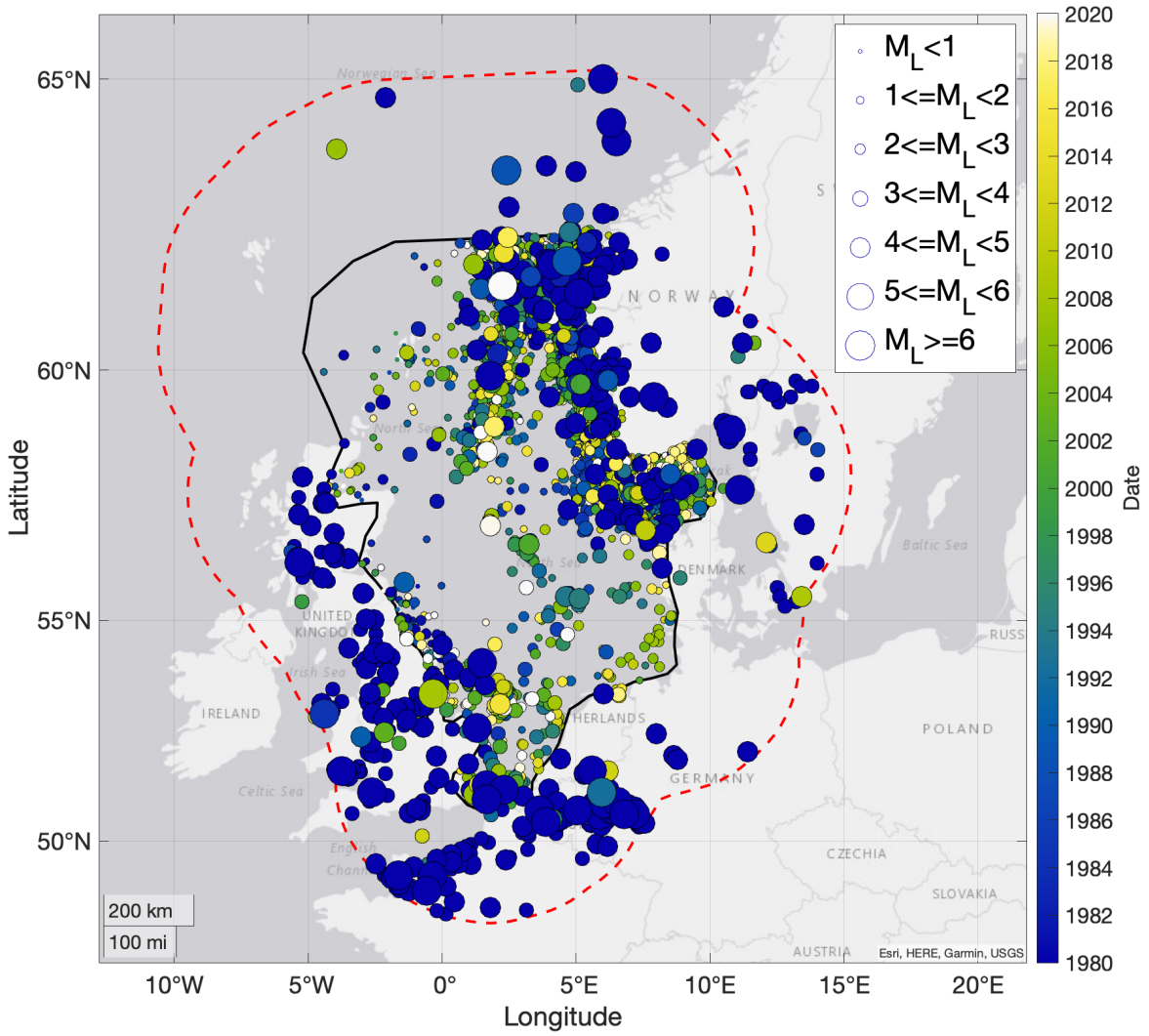

FIGURE 15: Map showing the expanded version of the North Sea catalogue intended for seismic hazard analysis. Events are sized by magnitude and coloured by occurrence time since 1980. The black solid line shows the original North Sea polygon used for discriminating events that are of primary interest to the SHARP project, while the red dashed line shows the expanded region.

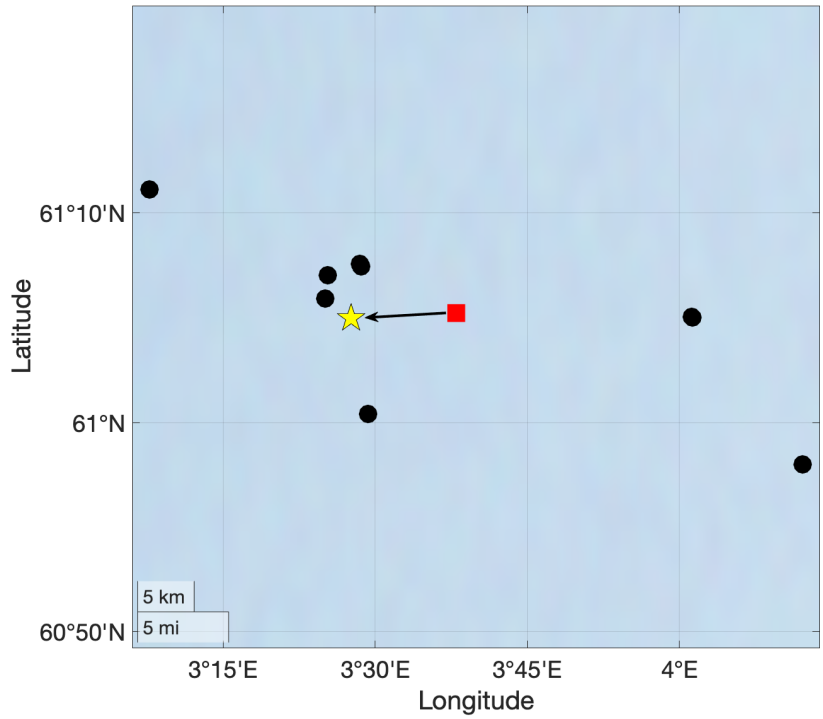

FIGURE 16: A schematic showing the routine to select "prime" locations in the earthquake bulletin. Events origins (occurrence times and locations) are shown by the black circles. The circular mean of the locations is shown as the red square. The closest origin to this mean location – and thus the prime origin – is shown by the yellow star. This plot uses data from an example $M_L \sim 3$ event that occurred on June 27th 2005 at 18:46:37.

1. The circular mean of the epicentres (i.e., latitudes and longitudes) in the origin block is calculated.
2. The prime origin is chosen to be the origin for which the epicentre is closest to the mean epicentre.
3. Prime magnitudes are selected first from those which are associated to the prime origin.
4. Other magnitude types not associated with the prime, but still present in the bulletin, are included. The median of the values that is present for each magnitude type is chosen as the prime for each magnitude type.

This routine is shown graphically in Figure 16 This does change both the locations and magnitudes of the prime catalogue, and thus any workflows that use the prime catalogue data must also be updated. This routine weights all origins equally, and doesn't take into account the quality of the input data used in their computation. This method aims more to capture and represent the uncertainty in the provided locations.

2 Event relocation

After cleaning the seismic event bulletin from double entries (see section 1.1) and obvious non-tectonic events (see section 1.2), all events in the new bulletin, which exhibits a completeness achieved never before for the North sea area, are ready to be relocated to improve the accuracy of epicentre and depth estimates.

2.1 Stations and station distribution

A thorough effort was made to identify as many station coordinates in the bulletin as possible. The bulletin includes phase readings from 2,620 unique seismic stations, with their distribution depicted in the upper section of Figure 17.

There is a dense concentration of stations in the United States and Europe. Notably, in the United States, phase readings are included only for larger-magnitude earthquakes. The lower part of Figure 17 highlights the stations around the North Sea. Different colours are used to indicate the number of phase readings provided by each station in the bulletin. A significant number of phase readings come from onshore stations in Norway, likely reflecting the seismicity pattern in the area, with a higher frequency of earthquakes occurring in the Norwegian sector of the North Sea

Figure 18 provides the statistical distribution of the number of unique stations listed for each event in the bulletin. Events with zero stations are historic events documented only through macroseismic records. Typically, events registered on only two stations are explosions.

2.2 Earthquake relocation

To relocate the seismic event catalogue for the European Arctic, we followed a previously used procedure (Schweitzer et al., 2021), which involved applying the HYPOSAT algorithm (Schweitzer, 2001) to determine the source parameters. HYPOSAT leverages the Generalised Matrix Inversion algorithm (Menke, 2018). In line with standard HYPOSAT procedures, we used all available data related to the seismic source location for the inversion process. This included onset times from local, regional, and teleseismic phase readings, as well as back azimuth, ray parameter (slowness), and travel-time differences between phases recorded at the same station.

We excluded T-phase readings, long-period surface waves, and infrasound readings from our relocation due to the typically high uncertainties associated with these types of phases. For our relocation, we used the following parameters and criteria:

- To ensure reliable event locations, we focused on seismic events that were registered on more than five stations. This approach resulted in the inclusion of 7,089 events (see Figure 18).
- We consider only stations within a 10° radius around the earthquake epicentre to ensure a sufficient number of stations for a stable solution, excluding phase onsets from distant stations that may disturb the inversion.
- To calculate realistic location uncertainties, the standard HYPOSAT uncertainties for the travel-time tables (model uncertainties) are employed. For P-type onsets, the theoretical travel times are assumed to have a mean uncertainty of 0.5 seconds, and for S-type onsets, 0.87 seconds.

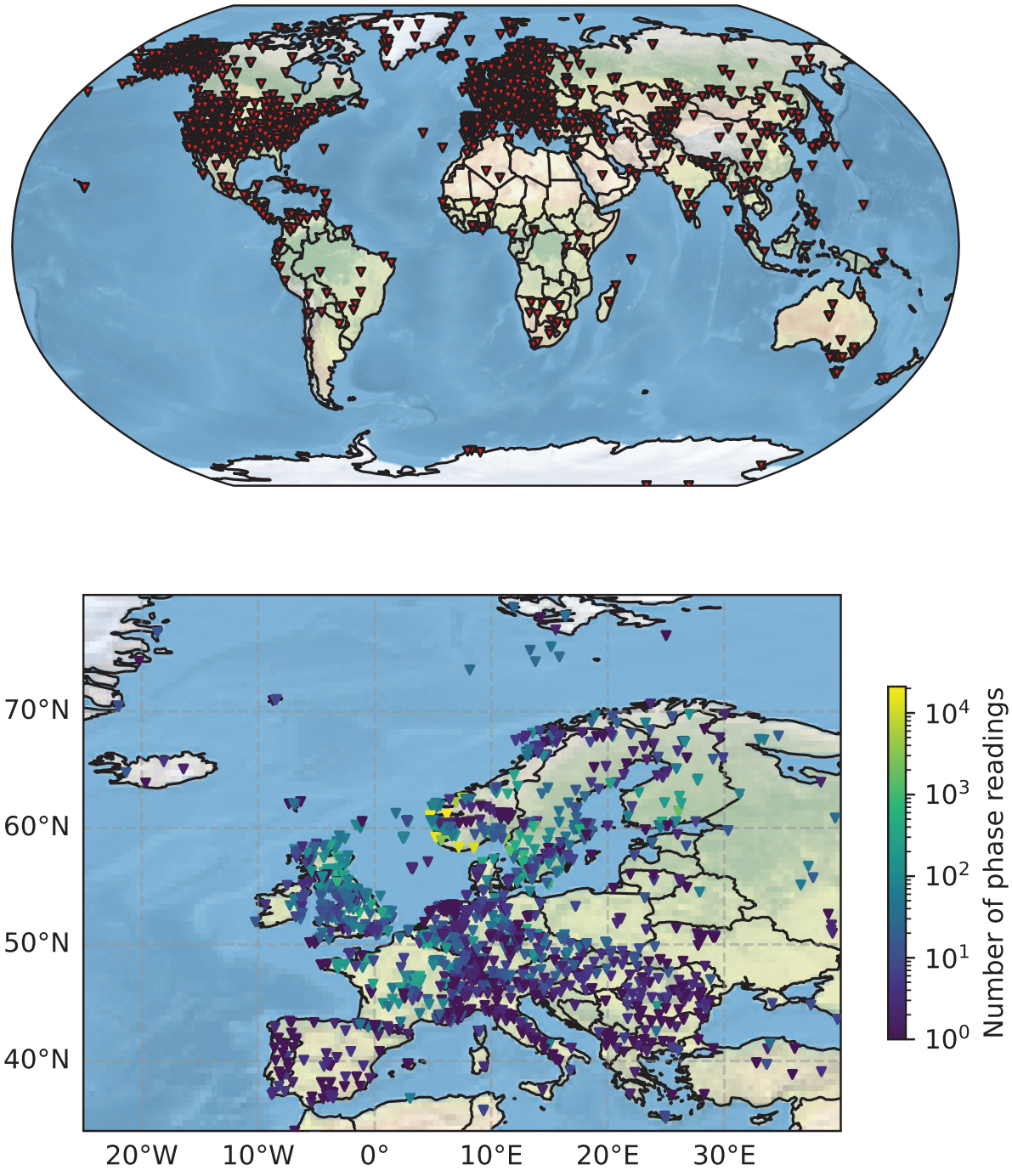

FIGURE 17: Seismic stations with phase readings in the bulletin. The top panel displays the global distribution, while the lower panel offers a zoomed-in view of Europe. Different colours represent the number of phase readings included from each station in the bulletin.

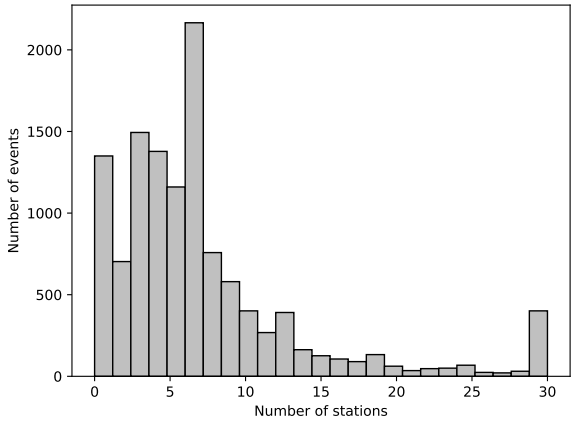

FIGURE 18: Distribution of the number of unique seismic stations used to locate seismic events comprised in the new North Sea bulletin. All events registered on more than 30 seismic stations are gathered in the last column.

Station elevation corrections are calculated based on the observed phase type and the theoretical ray parameter of the onset, with values of 5.8 km/s for P-type onsets and 3.46 km/s for S-type onsets.

Determining the best travel time table set for locating seismic events in the North Sea can be challenging due to sparse station coverage, significant variability in crustal structure, and limited near-source observations. Studies by Hicks et al. (2004), Schweitzer and Kennett (2007), and Gibbons et al. (2016) have shown that seismic epicentres can shift considerably when different travel-time models are used. In this study, we initially locate seismic events using the FESCAN velocity model (Mykkeltveit and Ringdal, 1981). For more information on why we chose this model and additional studies on velocity model testing, we refer to our paper (see below).

Further, there is a large trade-off between source time and source depth in the region due to missing near-source observations (e.g., Stange and Schweitzer, 2004; Schweitzer and Kennett, 2007; Havskov et al., 2012), leading to poorly constrained event depths. Therefore, the computation of rms depths may lead to unrealistically large numbers (deeper than the crustal thickness). Instead, to explore the potential depth range, all events were systematically relocated with depths fixed at 0 km, 5 km, 10 km, 15 km, 20 km, 25 km and at the default depth of the different source regions as used by the ISC (Bondár and Storchak, 2011) or, if this depth was not defined, in the middle of the crust, i.e., half the Moho depth as defined in CRUST1.0 (Laske et al., 2013) for the source region. Finally, the event depth from the best relocation result is selected.

After relocating the seismic events, we apply several criteria to remove significant outliers and ensure that only events with reliable location estimates are included:

- distance to the nearest station is smaller than 3°,
- magnitude greater than 1,
- station gap less than 300°,

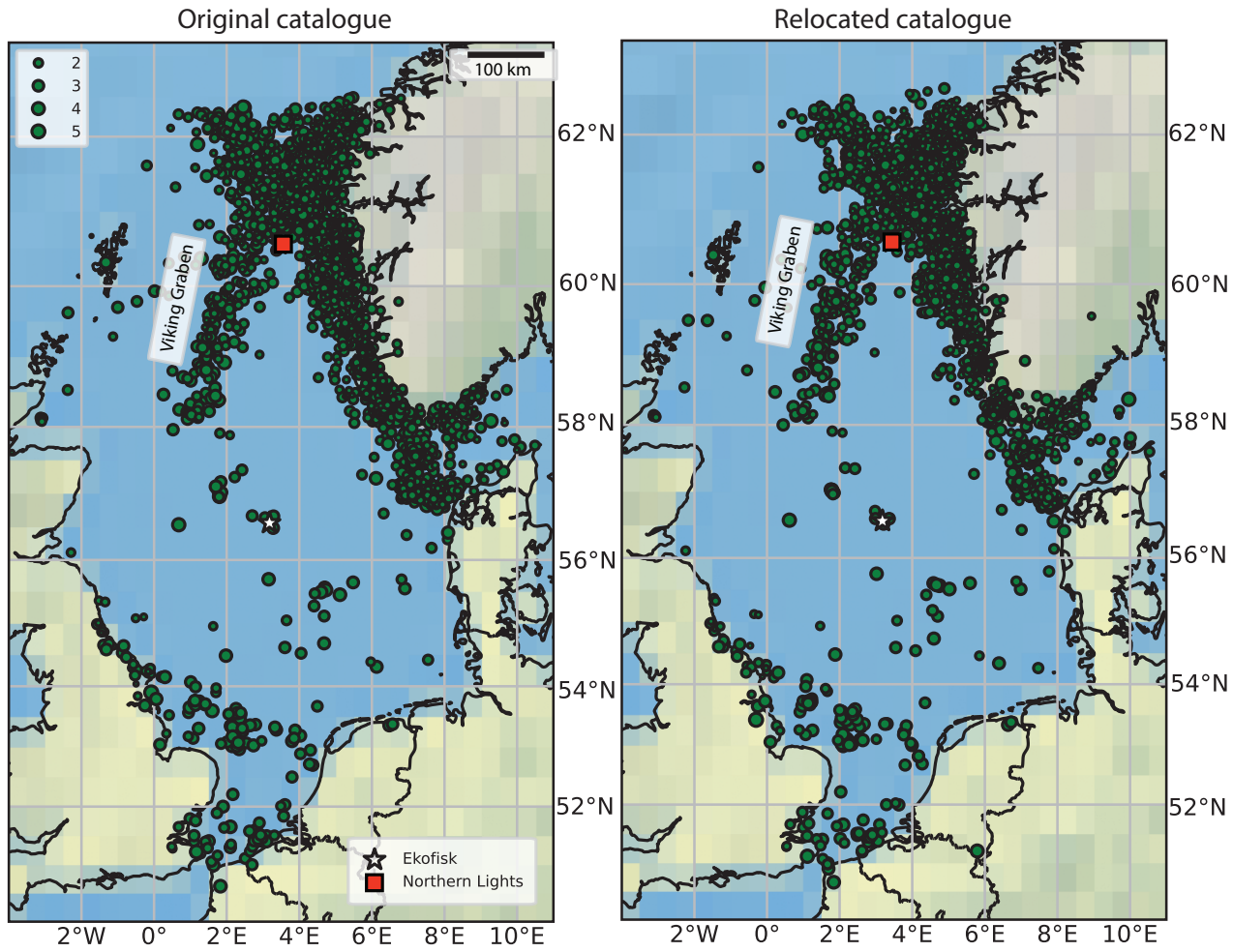

FIGURE 19: Event relocations. Left-hand panel: Event locations from the original bulletin. Right-hand panel: Event location from relocated bulletin.

- error ellipse area under 400 km^2,
- over 15 defining parameters utilised for the solution, and
- weighted RMS (ISC type) smaller than 1.5 s.

By applying these criteria, we included a total of 4,757 events in the final bulletin. The results, presented in Figure 19, indicate a more consistent seismicity pattern compared to the original bulletin. Earthquake density is high along the Norwegian coastline and in the Viking Graben, gradually decreasing towards the Central Graben. There is also a high density of earthquakes along the southeast coast of England and in the Skagerrak. Notably, there are two significant outliers onshore in Norway, which are most likely explosions with erroneous locations in the original bulletin.

2.3 New epicentre uncertainty estimates

Simultaneously, we re-estimate the location uncertainties for the relocated events, since the initial uncertainty ellipses are underestimated; they do not account for uncertainties associated with the choice of the velocity model. We relocate all events using six velocity models from the suite of avail-

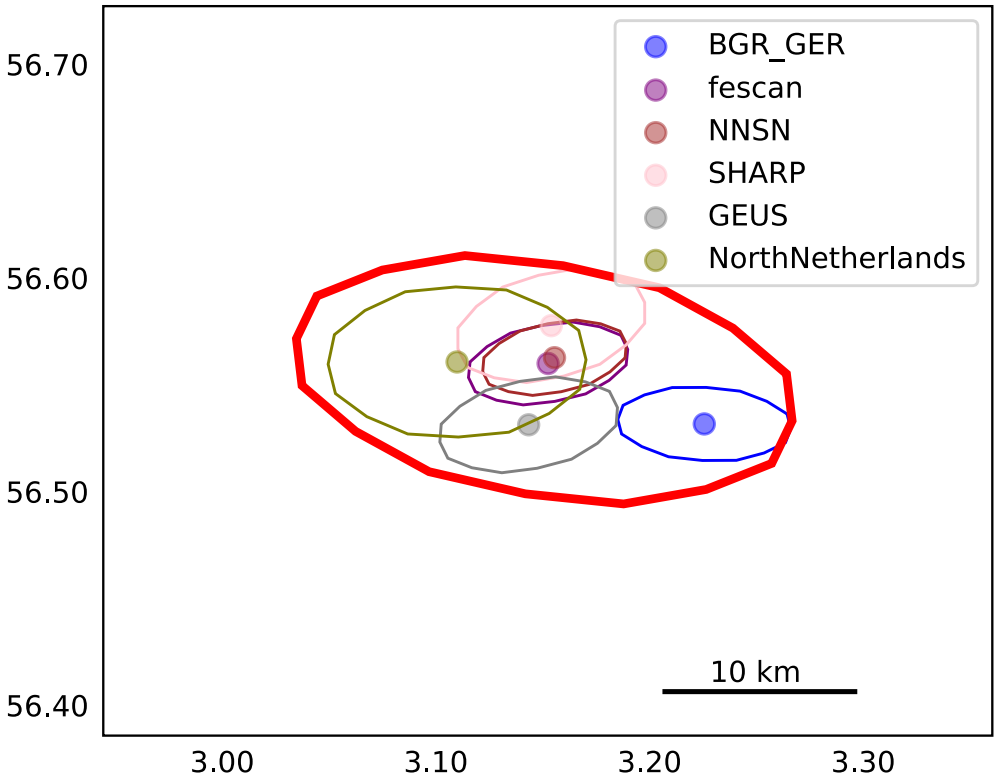

FIGURE 20: New epicentre uncertainty estimate. We relocated the M_w 4.3 Ekofisk event from 2001 using six different velocity models and plotted the corresponding uncertainty ellipses. Additionally, we created a new, larger ellipse that encompasses the area of all original uncertainty estimates. This encompassing ellipse is marked with a thick red line and serves as our new uncertainty estimate.

able models presented in deliverable D2.1 that best fit the regional characteristics. Subsequently, we plot the location and uncertainty for each event and adjust the uncertainty ellipse to comprise all uncertainty ellipses associated with the locations derived from the six different models. An example is shown in Figure 20 for the M_w 4.3 Ekofisk event in 2001. The figure displays the locations obtained when using the six different models, together with their associated ellipses. The newly fitted ellipse shown by a red line represents our new uncertainty estimate.

For more details on the relocation process and conducted testing, we refer to the manuscript "Relocating seismic events in the North Sea: challenges and insights for earthquake analysis" currently being prepared for submission to Geophysical Journal International.

3 Waveform repository

3.1 Publicly available data

During the progress of the project, it transpired that several tasks in both work packages WP2 and WP5 rely on the availability of waveforms for processing, for example moment tensor inversion, magnitude and stress drop computations, generation of a North Sea ground motion model and potentially, even the event relocation if a re-picking of arrival times becomes necessary. To avoid a duplication of work, a central waveform archive was established at NORSAR and data was made available to project partners with help of an FDSN web service (section 3.1.1). Data were downloaded from online sources, such as FDSN web services of various institutions, using the Squirrel tool of the pyrocko software package (section 3.1.2, Heimann et al., 2017). Please note that the quality of neither waveform data nor station metadata could be evaluated within this project. Instead, users of the waveform archive are responsible to perform quality checks before employing the data in their analyses.

3.1.1 FDSN web service

The International Federation of Digital Seismograph Networks (FDSN, https://www.fdsn.org/) is a global organisation. Its membership is comprised of groups responsible for the installation and maintenance of seismographs either within their geographic borders or globally. Members agree to coordinate station siting and provide free and open access to their data. In addition, network codes are assigned by the FDSN in order to provide uniqueness to seismological data streams. The FDSN was also instrumental in development of a universal standard for distribution of broadband waveform data and related parametric information. The Standard for Exchange of Earthquake Data (SEED) format is the result of that effort.

FDSN web services define standards for providing seismic and related data over the web. SEED (for station metadata and waveforms) and FDSN StationXML (for station metadata) are standardised data formats used for such data exchange. The project-internal FDSNWS server providing the FDSN web service was set up using the SeisComP software (Helmholtz-Centre Potsdam - GFZ German Research Centre for Geosciences and gempa GmbH, 2008) without requiring a full SeisComP installation.

3.1.2 Algorithm for data download

We compared different software tools for automatic data download, most notably the ObsPy (Beyreuther et al., 2010) massdownloader (https://docs.obspy.org/packages/autogen/obspy.clients.fdsn.mass_downloader.html) and the pyrocko (Heimann et al., 2017) Squirrel code (https://pyrocko.org/docs/current/topics/squirrel.html). Both codes automatically contact different data providers and do not require knowledge which data is available from which server. In addition, data is downloaded only once and potentially availablity of data from multiple providers is taken care of. The main disadvantages of the massdownloader are that

- it has no functionality for querying the database,
- the SeisComP database structure required for the FDSN web service has to be built manually, and
- additional data obtained in other ways (for example non-public data from agencies) has to be

added manually.

The massdownloader may be slightly easier to use, but the rich functionality and effective data handling of the Squirrel prevail. The operating mode of the Squirrel application is described in more detail in the appendix (A, pp.59).

3.1.3 Parameters for data download

Criteria for downloading waveform data from earthquakes were chosen as follows:

- years 1990-2022;
- prime magnitude given in the bulletin $M_{prime} \geq 3.5$ (smaller or larger local magnitudes may have been reported in subsequent entries);
- priority channel list: 'HH?', 'BH?', 'HL?', 'BL?', 'MH?', 'SH?', 'EH?', 'ML?', 'SL?' and 'LH?', where the question mark is a placeholder for the 3 components of the stations, which may be specified as E, N, Z or 1, 2, 3 or a combination thereof;
- for networks BE (Royal Observatory of Belgium, 1985), DK (Seismisk Tjeneste, 2023), GB (BGS, Great Britain), GR (Federal Institute for Geosciences and Natural Resources, 1976) as well as Norwegian networks NO (NORSAR, 1971) and NS (University of Bergen, 1982) as well as the temporary Scandinavian network Z6 (Weidle et al., 2010), download data from all available stations;
- only download data for selected stations from the Dutch NL network (Royal Netherlands Meteorological Institute (KNMI), 1993), namely stations DBN, HGN, OPLO, WTSB, WIT, SL014, NH014, OTLT, OTL4, PPBT, PPB4, WHMT, WHM4, ZH024, ZH034, ZH044, T064, T084, FR044, FR054, GK014, N034, G81B, G82B, G83B, G84B, G114, G124, G274, G604 in order to avoid a data download from the huge Groningen network;
- only download data for selected stations from the GEOFON network GE (German Research Centre for Geosciences GFZ, 1993), namely stations KBS, PUL, VSU, SLIT, PBUR, PABE, VAL, DSB, ILTH, MTE, MATE, MARCO, TIRR, WLF, STU, MORC, IBBN, FALKS, FLT1, RUE, RGN, HLG, in order to avoid a data download from globally distributed, far away stations;
- request data from the following FDSN sites: AusPass, BGR, ETHZ, GEOFON, KNMI, KOERI, ICGC, INGV, IRIS, IPGP, LMU, NOA, ORFEUS, USP and the Eida node of the University of Bergen.

In addition, waveforms from the KQ network (Christian Albrechts - Universitat zu Kiel, 2017) were delivered to NORSAR as soon as stations became available.

3.2 Waveform archive for the greater North Sea region

In order to gain an overview on the completeness of the waveform download, waveforms in the archive were compared to stations mentioned in the bulletin. The comparison was performed event by event, but only for networks we requested data from. However, this means that this comparison also excludes data that may have been requested but was not used for the bulletin.

Figure 21 gives an overview on the waveform data downloaded for the greater North Sea, while Figures 22 and 23 show statistics on which waveforms could not be obtained online. Figure 21 left

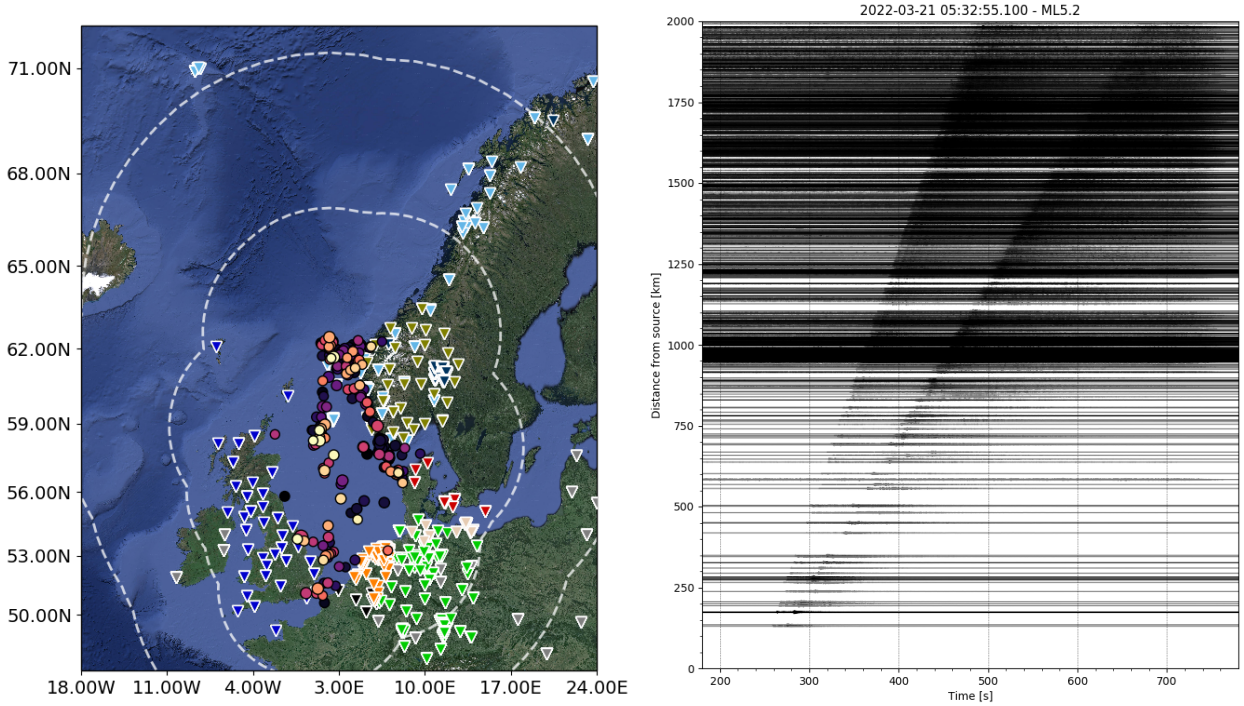

FIGURE 21: Left: events for which waveform data was requested (circles coloured by event occurrence time, the lighter the colour, the more recent the event) and stations from which waveform data was available (triangles coloured according to seismic network); right: example seismogram section for M_{L} 5.2 event on 21$^{\mathrm{st}}$ of March 2022

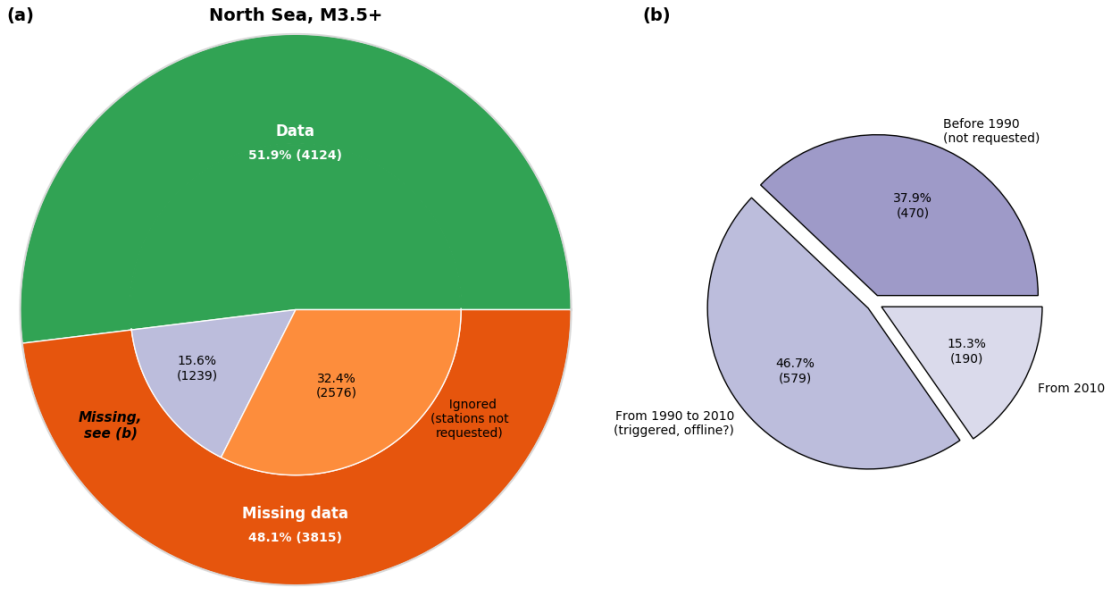

FIGURE 22: Comparison of downloaded waveform data with stations in the bulletin; left: data available in and missing from archive; right: separation of missing data

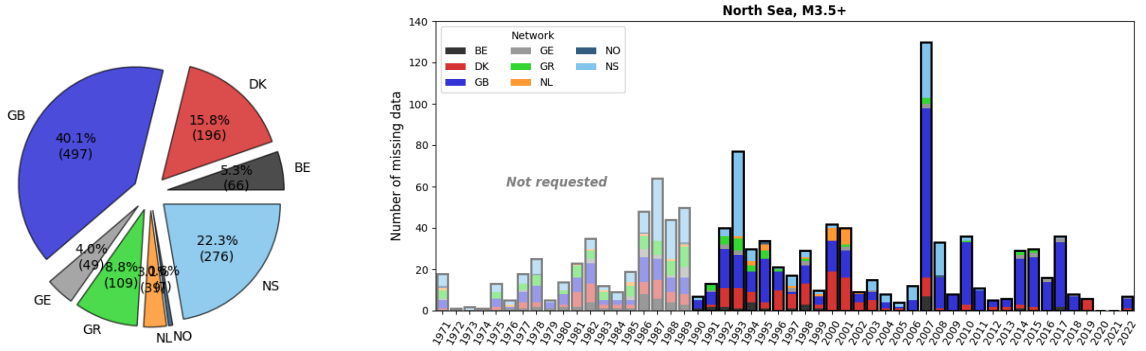

FIGURE 23: Pie chart (left) and histogram (right) of missing data differentiated after network

displays the 193 events resulting from the imposed temporal and magnitude restrictions together with the numerous stations from which waveform data were available. The high density of stations is also clearly recognisable from the seismogram section on the right. Only few stations are available to the North and Northwest, therefore, stations on the Orkney Islands, Shetland Islands, Faroe Islands and Jan Mayen are of particular importance to close the azimuthal gap.

Figure 22 left compares data available in the waveform archive after download with event-station pairs comprised in the bulletin. For 52% of these, waveform data was downloaded (green sector), consisting of 4,124 records. However, for 32% of the remaining station-event-pairs (red sector), data was not requested (orange sector), since stations do not belong to one of the networks mentioned above. Thus, only 16% of the data from the requested networks was not obtained (grey sector). This is analysed further in the pie chart to the right. From the missing 1,239 records, 38% were recorded before 1990 and were therefore not requested (dark grey sector). Of the remaining records, 579 belong to events occurring before 2010 (medium grey sector) and we suspect that these data are not available online. The cause of the remaining 190 records not being available is unclear (light grey sector). Figure 23 shows the networks the unavailable data was recorded in. It is visible that missing records are distributed unevenly throughout the years and that most of the missing records stem from the GB, NS and DK networks. Seismological agencies participating in this project aim to transfer missing waveforms, if available in-house, manually to NORSAR. Data from the NORSAR in-house archive has already been added to the waveform database, thus only a negligible amount of data remains undiscoverable for the NO network.

3.3 Waveform archive for the greater Horda platform region

The calculation of stress drops requires the availability of waveforms for a large magnitude range with sources evenly distributed in the region of interest and a good azimuthal coverage. Stress drop computations will therefore focus on a specific region, namely the Horda platform, instead of the larger North Sea area. However, due to the different requirements, additional waveform data was downloaded for events occurring on the Horda platform, invoking no magnitude limit. However, stations for which records were downloaded were chosen imposing a magnitude-distance limit, since small magnitude events will only be recorded with a reasonable signal-to-noise ratio up to a certain distance. In addition, since data need to be of very good quality for the foreseen analysis, we requested only data recorded after the year 2000.

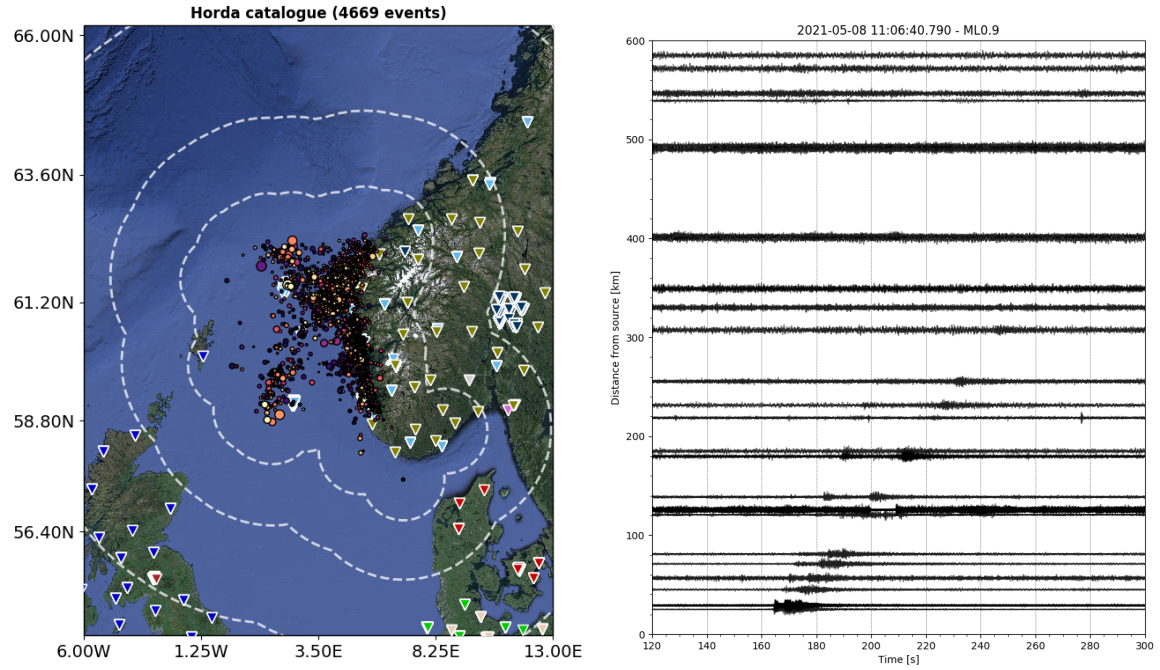

FIGURE 24: Left: events for which waveform data was requested and stations from which waveform data was available (see Figure 21 for explanation of symbols); right: example seismogram section for M_{L} 0.9 event on 8^{th} of May 2021

Figure 24 gives an overview on the waveform data downloaded for the Horda platform area, while Figure 25 and 26 show statistics on which waveforms could not be obtained online. The omission of the magnitude limit leads to waveforms of a much larger number of events being requested for the Horda platform area compared to the greater North Sea, namely 4,669 events. However, due to the smaller magnitude events not being recorded with sufficient quality at larger distances, the number of stations for which waveforms are available for each event is substantially smaller, as is also visible from the seismogram section to the right. Specifically, this results in a large azimuthal gap towards the Northwest, which may have negative implications for the application of certain analysis methods.

Figure 25 left compares again data available in the waveform archive after download with event-station pairs comprised in the bulletin. For 86% of these, waveform data was downloaded (green sector), consisting of 33,914 records. However, for 8% of the remaining station-event-pairs (red sector), data was not requested (orange sector), since stations do not belong to one of the networks mentioned above. Thus, only 6% of the data from the requested networks was not obtained (grey sector). This is analysed further in the pie chart to the right. From the missing 2,305 records, 2,155 belong to events occurring before 2010 (medium grey sector) and we suspect that these data are not available online. The cause of the remaining 150 records not being available is unclear (light grey sector). Figure 26 shows the networks the unavailable data was recorded in. It is visible that records are mainly missing between the years 2002 and 2009 and that most of the missing records stem from the NS network, which is reasonable, since this is the network closest to the Horda platform area and will thus have recorded more small magnitude events not visible on the other networks. Seismological agencies participating in this project aim to transfer missing waveforms, if available in-house, manually to NORSAR. Data from the NORSAR in-house archive has already been added to the waveform

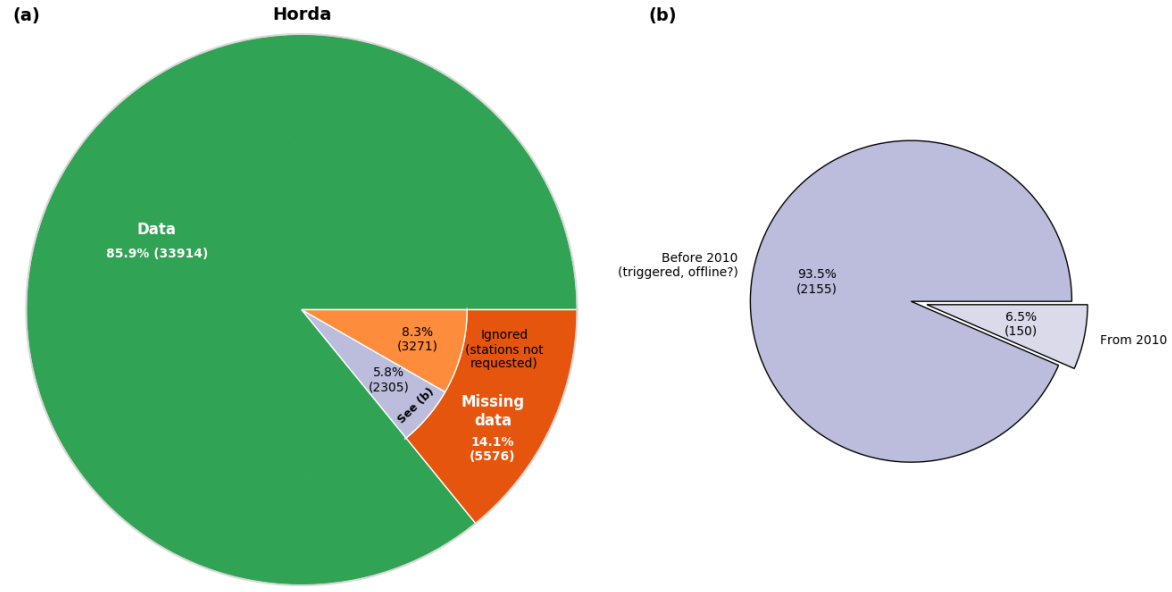

FIGURE 25: Comparison of downloaded waveform data with stations in the bulletin; left: data available in and missing from archive; right: separation of missing data

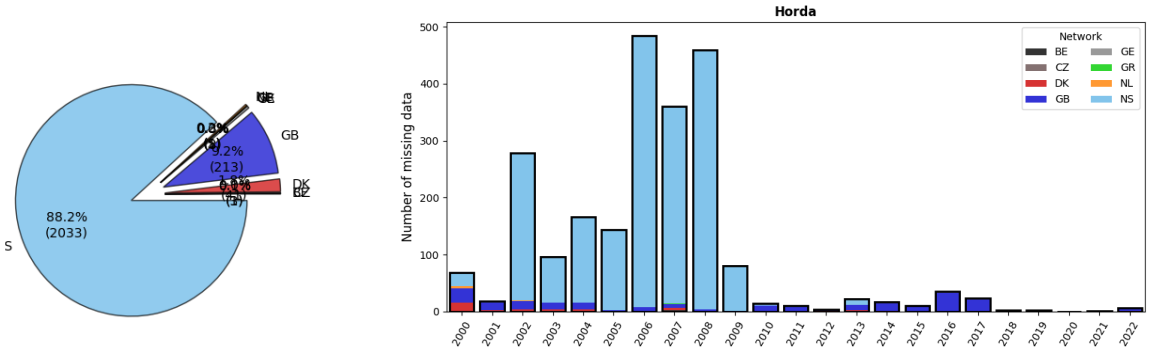

FIGURE 26: Pie chart (left) and histogram (right) of missing data differentiated after network

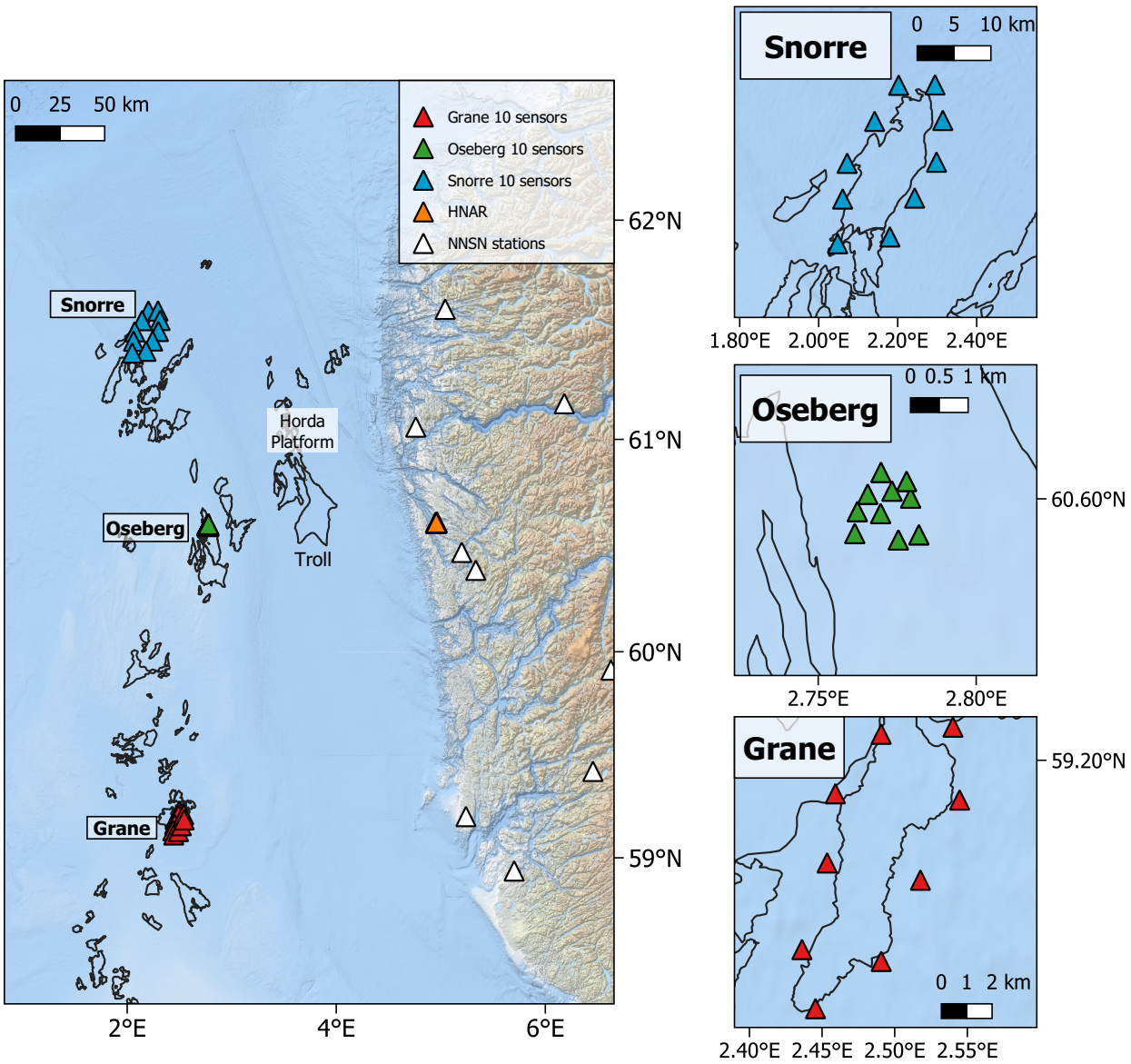

FIGURE 27: Offshore sensors (PRM nodes) provided by project industry partners; left: location of fields with respect to Norwegian coast, right: sensor distributions at Snorre (top), Oseberg (middle) and Grane (bottom) fields

database, thus only a negligible amount of data remains undiscoverable for the NO network. The NS network is maintained by the University of Bergen, which is not part of the project, though.

Available and missing data may overlap between both archives.

3.4 Data provided by industry partners

As a part of the SHARP project, we gained access to datasets from 10 handpicked sensors from the Permanent Reservoir Monitoring (PRM) systems deployed at the Snorre, Oseberg and Grane field, all maintained and operated by Equinor (see Figure 27). The same data is shared with the Norwegian National Seismic Network.

Our data access to the Snorre field sensors starts in mid-March 2022. Interestingly, this data includes the largest recorded earthquake in the North Sea in the past 33 years, which occurred on 21 March

2022. The epicentre is estimated to be only a few kilometres away from the Snorre field making this data set particularly significant for constraining the earthquake location. The selected sensors are placed along the rim of the Snorre field. For the Oseberg sensors, we received continuous data from September 2019 on. Unfortunately, these sensors were permanently switched off in August 2022. Unlike the sensor configurations at the other fields, the Oseberg sensors are densely spaced such that they are suitable for array processing. From the Grane sensors, we obtained continuous data dating back to April 2018. As for the Snorre field, the 10 selected sensors are placed along the rim of the field to ensure optimal station coverage.

One of the most significant challenges when using this data for analysis is the significant amount of noise and data gaps. Seismic shooting is for instance often conducted during the summer periods, which results in either the sensors being periodically turned off or continuous spikes of noise within the data set making it challenging to pick clear phase arrivals.

4 Focal mechanism collection

As reported in the SHARP deliverable D2.1, we collected information to provide a catalogue of computed focal mechanisms as a base for comparison to the newly computed probabilistic moment tensors. Since this catalogue will be used for interpretation of the stress field, only high-quality data are included. Therefore, we restricted the catalogue to events after 1980 (starting with the year 1981), at which point the detection threshold in the North Sea had sunk considerably, see also section 5. The focal mechanism collection presented in deliverable D2.1 was now updated and the most important information will be repeated here.

The current collection contains focal mechanisms from the following providers:

- the Harvard CMT/GCMT catalogue (downloaded from: https://www.globalcmt.org/CMTsearch.html; see also Dziewonski et al., 1981b; Ekström et al., 2012);
- the ISC focal mechanism bulletin (downloaded from: http://www.isc.ac.uk/iscbulletin/search/fmechanisms/; see also Lentas, 2018; Lentas et al., 2019; International Seismological Centre, 2022);
- the GEOFON moment tensor catalogue (downloaded from: https://geofon.gfz-potsdam.de/old/eqinfo/form.php; see also Quinteros et al., 2021);
- the focal mechanism catalogues of countries bordering the North Sea delivered to NORSAR by:
  - BGS, United Kingdom;
  - GEUS, Denmark;
  - the Norwegian National Seismic Network (NNSN, https://nnsn.geo.uib.no), Norway. Since mechanisms may considerably vary in quality, only reviewed mechanisms published in Tjåland and Ottemöller (2018) were considered for now. A further collection by Tjåland (2020) only contains solutions of C and D quality, which were disregarded for now.

Further sources were checked, but did not record any focal mechanisms for events in the study area. The main additions in comparison to D2.1 are from the BGS focal mechanism catalogue. One further double entry in the collated catalogue was removed, since the event was reported by the ISC with author BGS as well as by the BGS itself:

- event on 23.01.2020 at 05:57:00 GMT.

Two further entries are very similar for the event on 09.06.2018 at 22:14:28 GMT, but since both event time as well as location are slightly different, both entries were kept, since theoretically, these entries may refer to separate events.

If several entries exist for the same event, entries were sorted using the following hierarchy: GCMT, NEIC, ISC, BGS, GEUS, NNSN, BER, GEOFON, MED_RCMT.

The resulting focal mechanism catalogue contains 70 entries describing presumably 54 (or 55) individual events. It is available as file accompanying this report and illustrated in Figure 28 and Figure 29. A comparison between the focal mechanism catalogue and the event bulletin (Figure 30) highlights

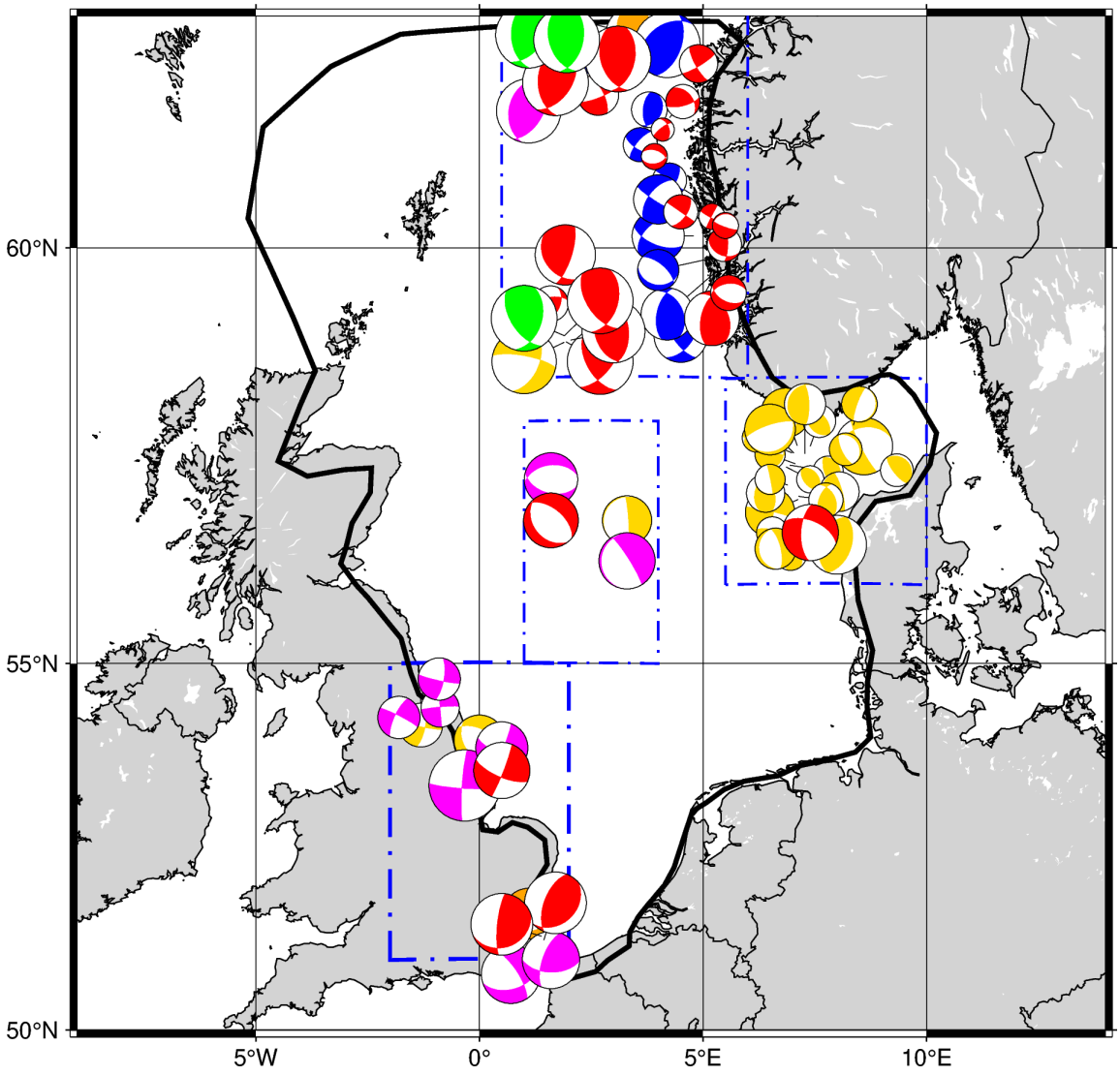

FIGURE 28: Prime entries for collected focal mechanism catalogue for the North Sea area. Colours mark reporting institutions: green – GCMT, red – ISC, magenta - BGS, yellow – GEUS, blue – NNSN, orange – GEOFON. Blue rectangles denote regions presented in more detail in the following figure. Mechanism sorted chronologically (more recent overlaying previous events) and hierarchically.

events for which it may be especially valuable to estimate moment tensors. This concerns for example regions exhibiting seismicity of which so far, no mechanisms seem to have been analysed (at least within the catalogues we considered) and large magnitude events, for which no mechanisms are available yet.

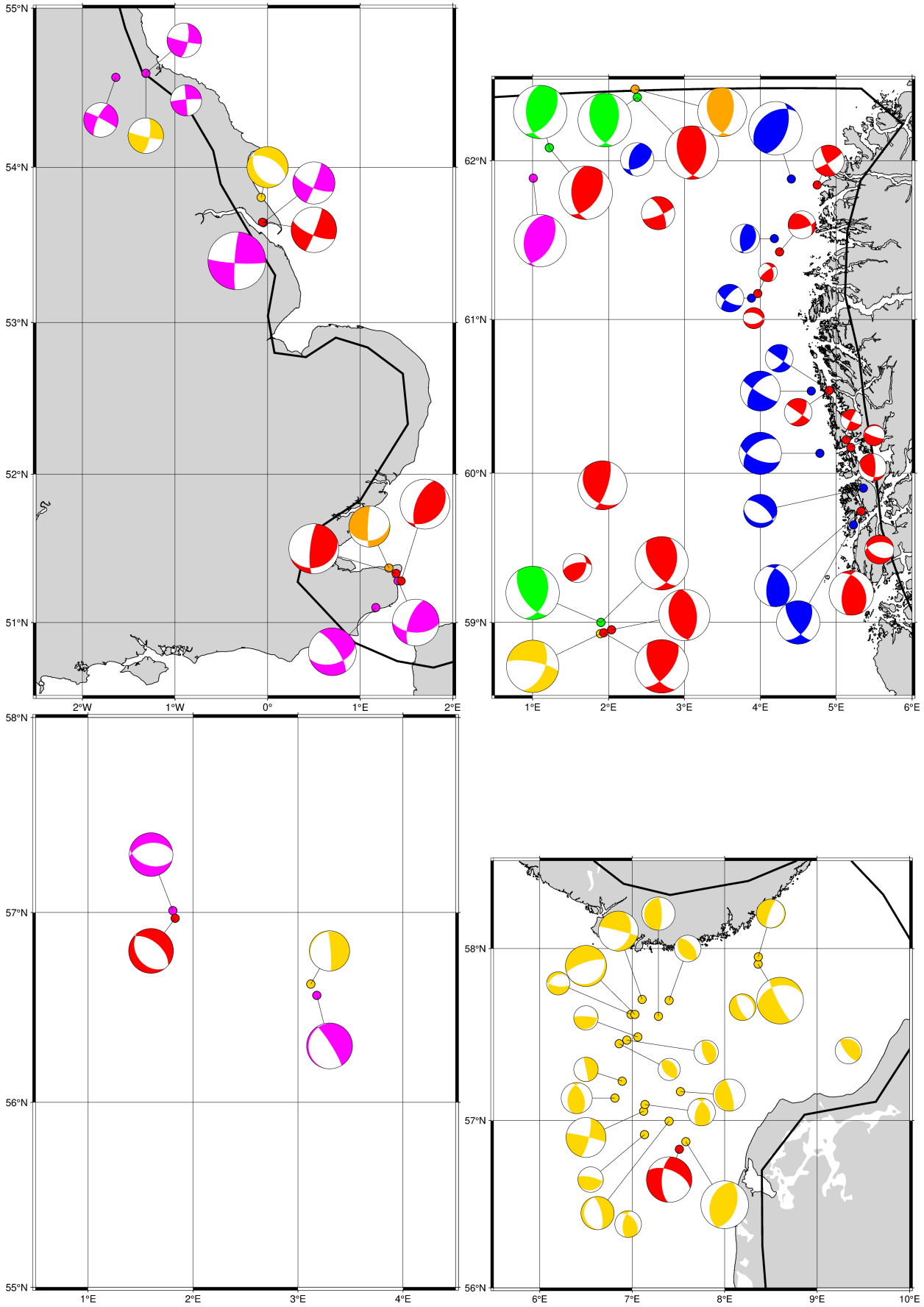

FIGURE 29: Zoom onto UK south coast (top left), Norwegian west coast (top right), central North Sea (bottom left) and Skagerrak (bottom right). See Figure 28 for explanation of colours.

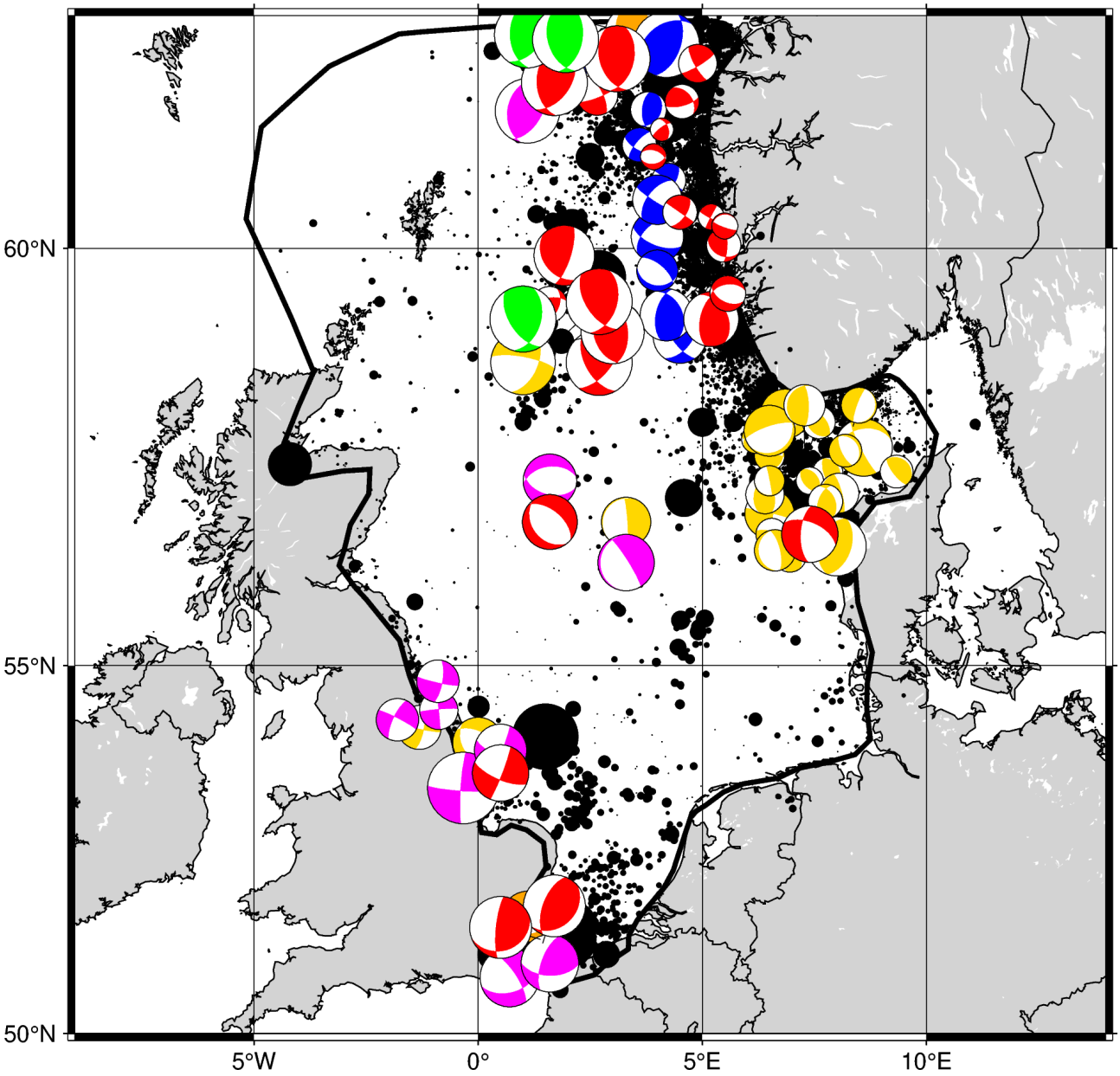

FIGURE 30: Comparison between focal mechanism catalogue (see Figure 28 for explanation of colours) and primary entries in event bulletin displayed as black dots sized according to magnitude. Mechanism sorted chronologically and hierarchically.

5 Moment tensor inversion

5.1 Data availability

The waveforms downloaded using the routine described in section 3 were employed for the analysis of the ability of this combined seismic network to characterise earthquake source mechanisms and, as a result, provide information on in-situ stress conditions.

As a first step, spatial distribution and azimuthal coverage were studied. Events recorded in the 1990s (Figure 31a) show very limited station coverage, mainly from the GR network (Federal Institute for Geosciences and Natural Resources, 1976) located in northern Germany, with a few additional stations from DK (Seismisk Tjeneste, 2023), GE (German Research Centre for Geosciences GFZ, 1993) and NL (Royal Netherlands Meteorological Institute (KNMI), 1993) networks. Starting from the late 1990's to early 2000's, stations from NO (NORSAR, 1971) and NS (University of Bergen, 1982) networks appear on the station coverage maps (Figure 31b). In the period of 2006 to 2008, a temporal network Z6 (Weidle et al., 2010) was deployed in Scandinavia (Figure 31c and 31d). In addition, some stations from the Belgian Seismic Network (BE, Royal Observatory of Belgium, 1985) start to appear on the maps in 2006. Starting in 2008, broadband stations were installed within the Great Britain Seismograph network (GB, British Geological Survey (1970)), providing coverage in the UK (Figure 31d). Beginning in 2015 (Figure 31e and Figure 31f), the station coverage started to resemble the present day's configuration (Figure 32). One of the latest additions is the Kiel University Earthquake Monitoring (KQ, Christian Albrechts - Universitat zu Kiel, 2017) network, which started its operation in 2017 (Figure 31f).

It should be noted that these maps with the station coverage only indicate that waveforms are available for the event in question but do not specify whether the data quality is sufficient for any data analysis. Due to the significant azimuthal gap for the events before 2008, moment tensor analysis was currently only tested on events past this year. Based on preliminary quality analysis of the waveforms for selected events, the magnitude and location of the hypocentre play crucial roles in the detectability of the event. Events located in the central part of the North Sea, for instance, the earthquakes on the 22nd February 2020 (18:42:55 GMT) and 25th of March 2022 (04:56:36 GMT) with magnitudes of 3.6 and 3.4, respectively, are not detectable on the networks installed onshore.

5.2 Probabilistic moment tensor inversion

The limited availability of waveform data and station distribution in the North Sea region requires the usage of a probabilistic approach for the moment tensor estimation, which will allow for uncertainty estimations of the retrieved source parameters. For moment tensor computations, we used open-source software Grond (Heimann et al., 2018).

Based on data analysis and methodological tests, we computed deviatoric moment tensor (MT) inversions for the selection of the events. By doing so, we hope to resolve a stable double-couple (DC) component of the moment tensor, with some erroneous parts in the compensated linear vector

[0]Data availability is based on the waveform download described in section 3 with the limitations described in subsection 3.2.

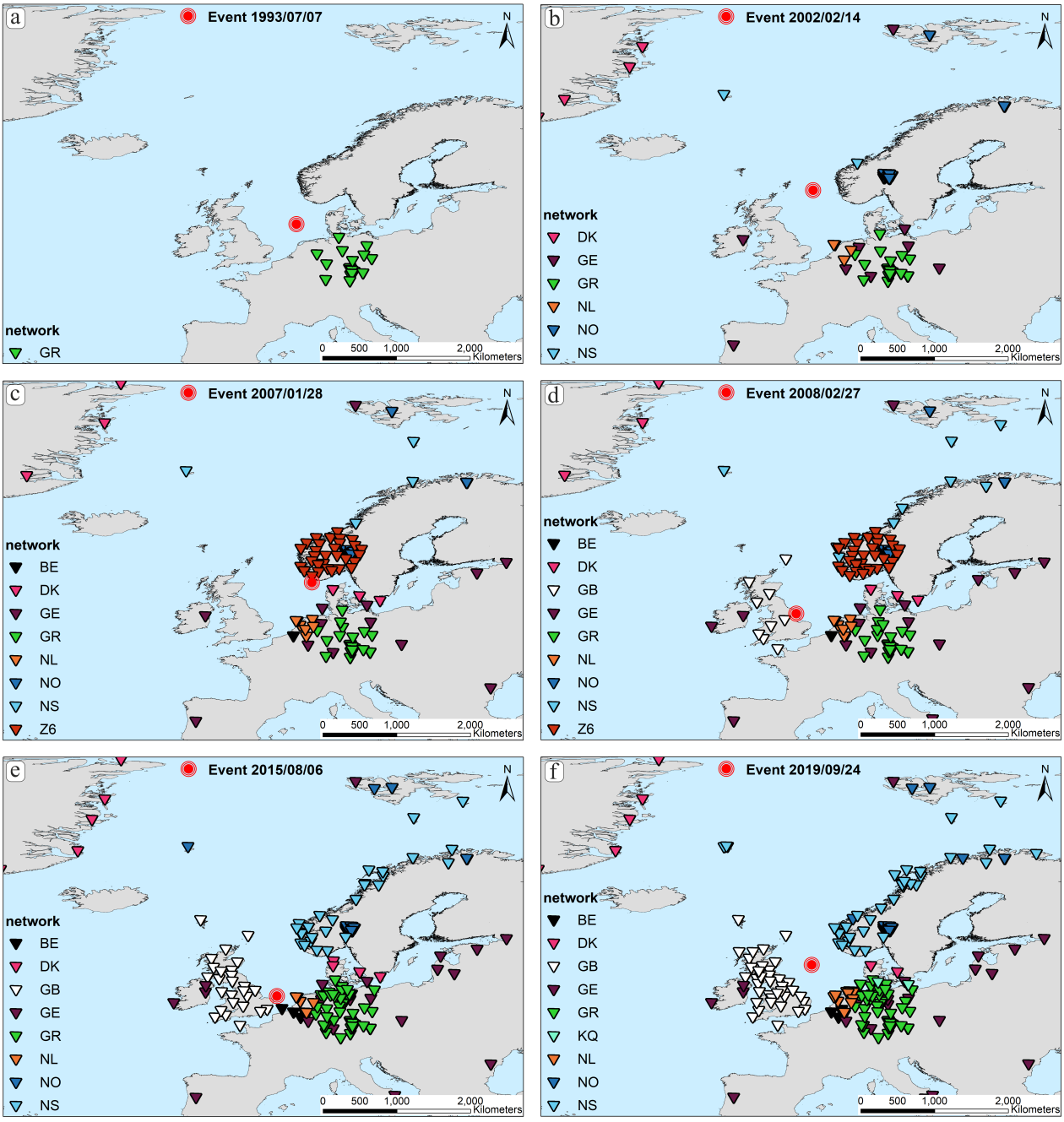

FIGURE 31: Maps of the seismic stations with available waveforms for the events on (a) the 2nd of June 1993 (10:37:48 GMT), (b) the 14th of February 2002 (19:00:38 GMT), (c) the 28th of January 2007 (10:30:53 GMT), (d) the 9th of October 2016 (12:48:30 GMT) (e) the 6th of August 2015 (15:03:59 GMT) and (f) the 24th of September 2019 (13:38:14 GMT).

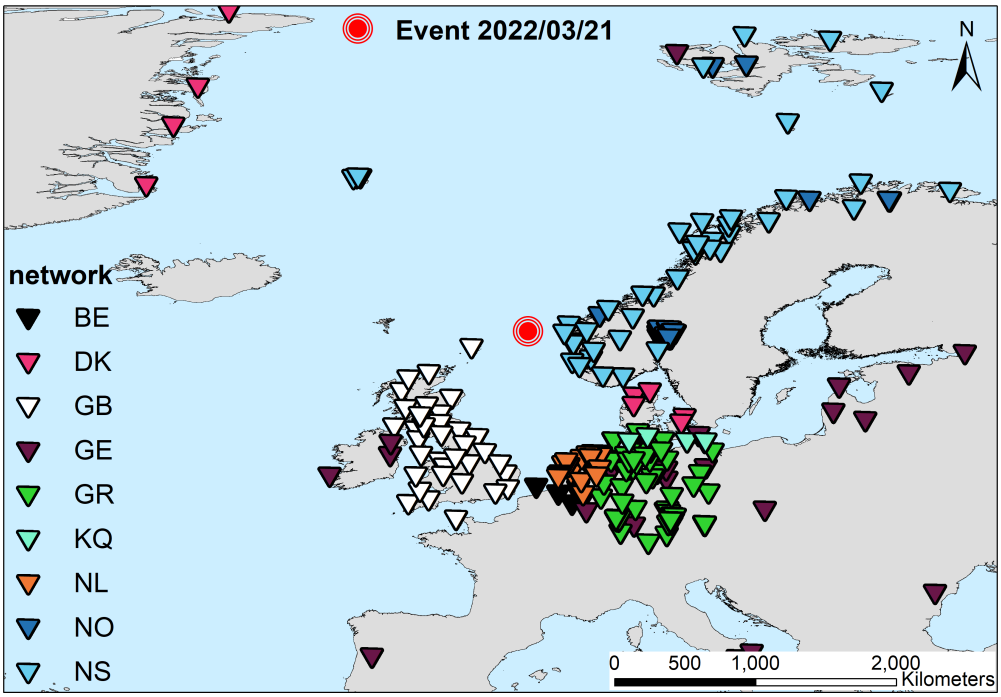

FIGURE 32: Map of seismic stations with available waveforms for the event on the 21st of March 2022 (05:32:55 GMT)

dipole (CLVD) component due to inversion artefacts. It should be noted that the deviatoric solution excludes mechanisms with a volumetric change in source.

The Grond algorithm uses forward modelling of numerous potential solutions instead of directly attempting to invert for the source parameters. Synthetic seismograms (forward simulation on Figure 33) are compared to observations of the target earthquake (observed displacement on Figure 33), and the procedure is iterated for different moment tensor configurations using a Bayesian bootstrap optimiser to retrieve an optimal moment tensor solution. The developed code efficiently navigates complex model spaces, analyses the trade-offs and uncertainties of source parameters and allows for probabilistic methodology and error estimations. The latter is especially crucial for the later integration of information in further modelling of the response of reservoir and caprock to large-scale fluid injection over prolonged periods. More detailed information on the code implementation can be found in Heimann et al. (2018).

5.3 Input data

The moment tensor inversion requires the following input data prepared in the right format: Green's function store (Figure 34a), waveform files in mseed format or other file formats supported by Pyrocko (Heimann et al., 2017) (Figure 34b), station files (Figure 34c) and event files (Figure 34d). Green's functions (GFs) are commonly used to represent force excitation in wave propagation and electromagnetic, mechanical, and thermal problems. For Green's function calculations, we used a 1D velocity model (Figure 35) derived from CRUST1.0 (Jerkins et al., 2023). The computation was performed using the Fomosto QSEIS code (Heimann et al., 2017; Wang, 1999). The filtered and windowed waveforms with reasonable data quality as well as the corresponding station files containing instrument responses

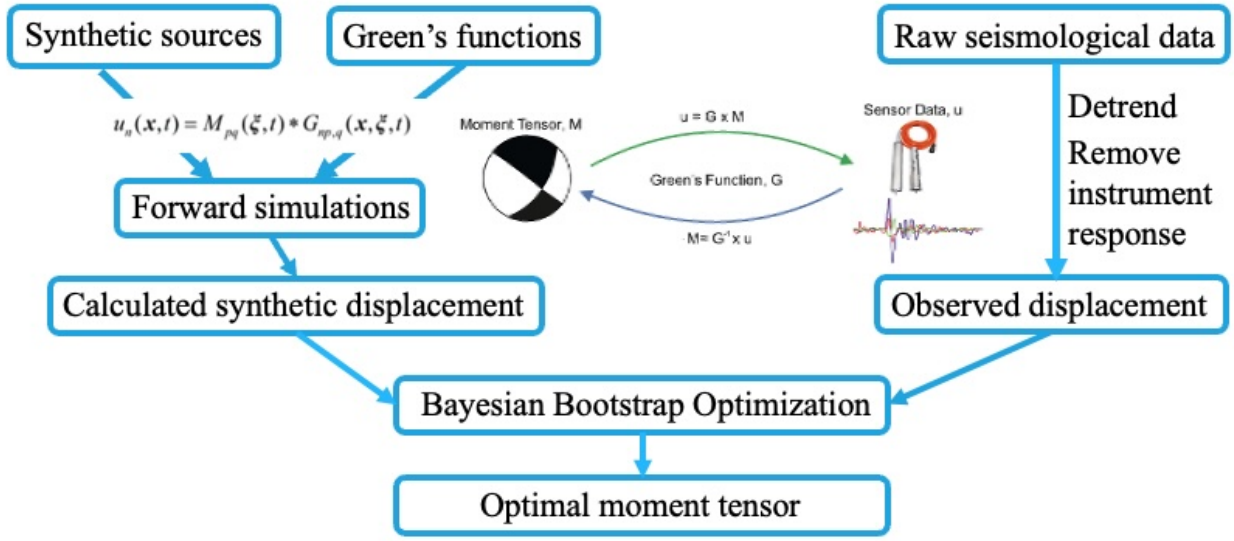

FIGURE 33: The principle of the bootstrap-based probabilistic Grond (Heimann et al., 2018) moment tensor optimisation code.

are used for data fittings during the optimisation process. The event files, containing information on the time of the event, coordinates of the hypocentre (latitude, longitude), magnitude and depth were created using the information listed in the newly created North Sea bulletin.

5.4 Moment tensor inversion parameters

Moment tensor (MT) inversion is particularly challenging for small to moderate-magnitude events due to the modelling problem of the relatively high frequencies. In addition, local site and topographic effects create difficulties in conducting full moment tensor inversion using 1-D velocity profiles at frequencies exceeding 0.1 Hz (Petersen et al., 2021). Seismic stations used for this study are positioned on land, surrounding the North Sea. In some cases, the distance between the location of the earthquake and the recording station can be more than 1500 km (see Figure 31). Furthermore, the signal-to-noise ratio varies significantly not only between the different seismological networks, but also from station to station within one network. Due to all these factors, we chose to perform a regional centroid moment tensor inversion using surface waves.

To test the moment tensor inversion parameters, we selected the earthquake that occurred on the 21st of March 2022, which has the largest magnitude (M 5.1, Jerkins et al., 2023) and the best station coverage (Figure 32), to reduce the effects related to spatial and azimuthal coverage. First, we started our analysis with the examination of the filtered (0.01-0.05 Hz) 3-component data (Figure 36) and locating the surface waves in the recorded time series. Rayleigh waves are characterised by an elliptical motion, producing both a vertical and horizontal component of motion in the direction of wave propagation. The movement of particles in fundamental mode Rayleigh waves is typically elliptical and thought to be retrograde on the surface (Shearer, 2019). We used an open-source Python package, TwistPy (Toolbox for Wavefield Inertial Sensing Techniques Sollberger, 2023), to perform a polarisation analysis and calculate ellipticity attributes. The elliptically polarised parts of the signal (e.g., surface waves) show a high degree of polarisation (larger than 0.7; Figure 36). This allows us

ⓐ Greens function store:

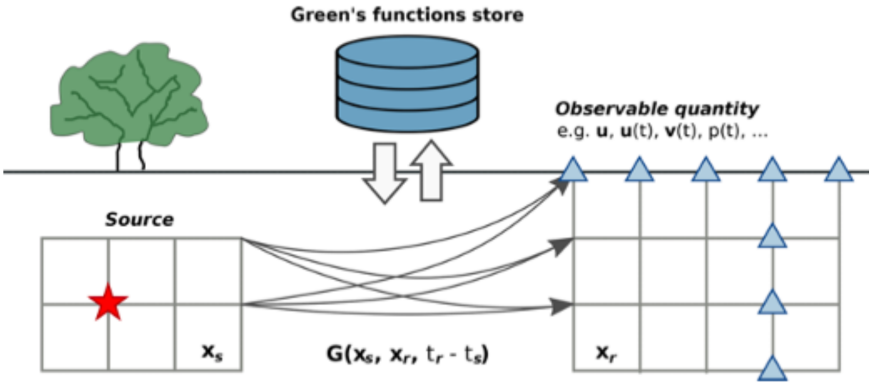

Heinmann et al. 2019

ⓑ Waveforms:

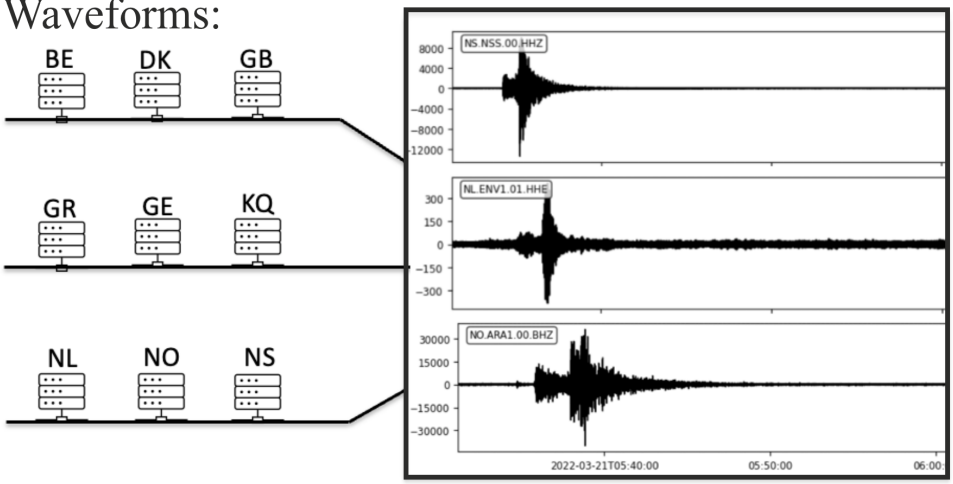

ⓒ Station Files:

```
<?xml version='1.0' encoding='UTF-8'?>
<FDSNStationXML xmlns="http://www.fdsn.org/xml/station/1" schemaVersion="1.2">
  <Source>Generated by Pyrocko Squirrel.</Source>
  <Module/>
  <ModuleURI/>
  <Created>2024-02-22T17:21:32.321583Z</Created>
  <Network code="NO">
    <Station code="AKN">
      <Latitude unit="DEGREES">62.178299</Latitude>
      <Longitude unit="DEGREES">6.9974</Longitude>
      <Elevation>508.0</Elevation>
      <Site>
        <Name></Name>
      </Site>
      <Channel code="BHE" startDate="2009-11-01T00:00:00.000000Z" endDate="2013-01-17T10:35:00.000000Z" locationCode="">
        <Latitude unit="DEGREES">62.178299</Latitude>
        <Longitude unit="DEGREES">6.9974</Longitude>
        <Elevation>508.0</Elevation>
        <Depth>0.0</Depth>
        <Azimuth unit="DEGREES">90.0</Azimuth>
        <Dip unit="DEGREES">0.0</Dip>
        <SampleRate unit="SAMPLES/S">200.0</SampleRate>
        <Sensor>
          <Description>CMG-3E</Description>
        </Sensor>
        <Response>
          <InstrumentSensitivity>
            <Value>608698000.0</Value>
            <Frequency>1.0</Frequency>
```

ⓓ Event file:

```
name = event_2022-03-21_05-32-55
time = 2022-03-21 05:32:56.440
latitude = 61.53
longitude = 2.53
magnitude = 5.24
depth = 25000
```

FIGURE 34: The input files required for the probabilistic moment tensor inversion using Grond.

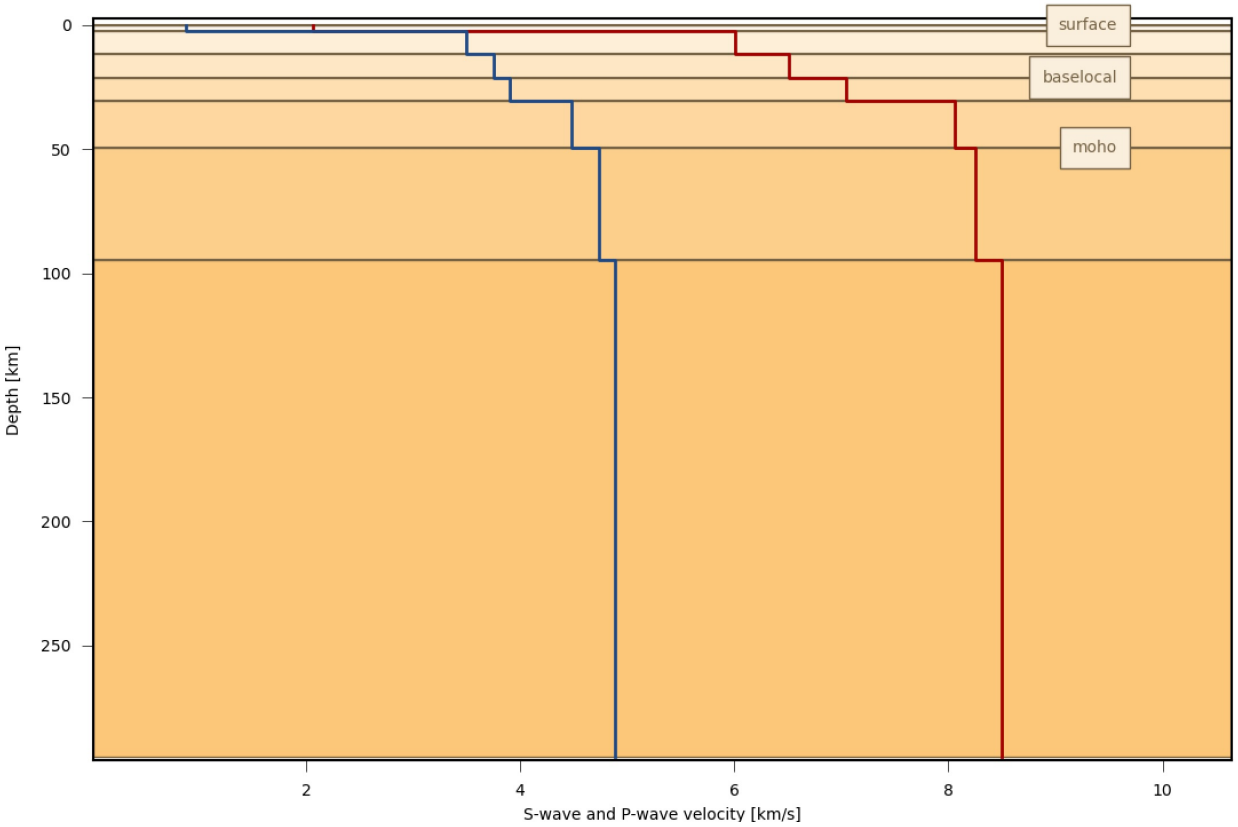

FIGURE 35: Velocity model used for Green's function computations (see supplement material in Jerkins et al., 2023).

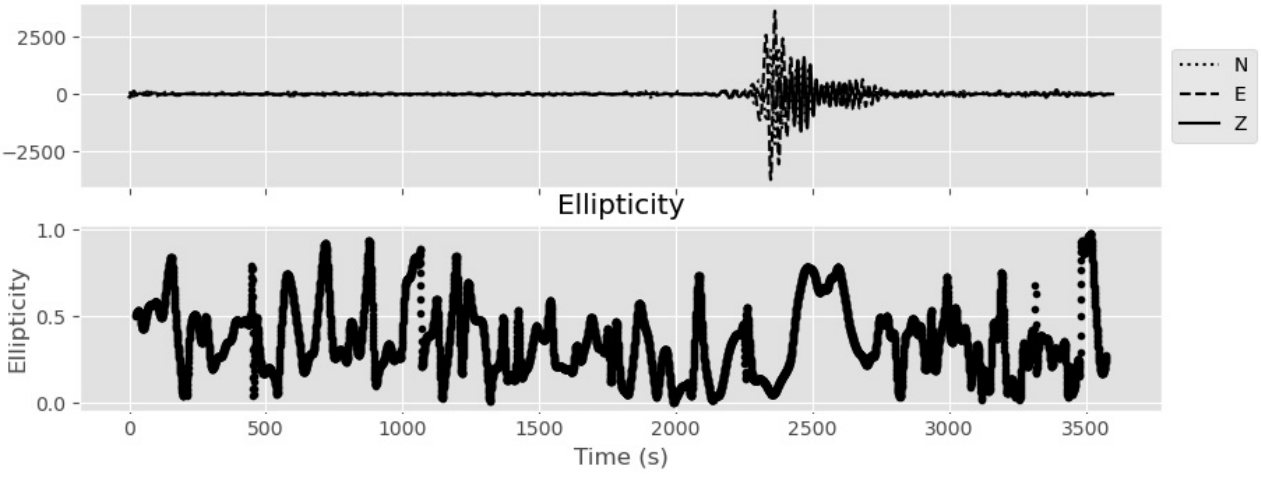

FIGURE 36: Ellipticity attribute computed using 3C data from ARA3 station of the NO network (NORSAR, 1971).

to locate the Rayleigh wave window within the wavetrain. Love waves have a particle movement in a horizontal plane perpendicular to the direction of propagation, causing the ground to move sideways with no vertical displacement. The solid line on Figure 36, corresponding to the vertical component, at the beginning of the surface wave window in the part where we observe the Love wave.

After parameters testing, the time window for data fitting was defined as follows: the start time was

chosen using the modelled P-wave arrival times, while the end time was calculated using the distance between the station and the earthquake location and an average surface wave velocity of 2.5 km/s.

Due to the heterogeneity of the dataset and errors found in a few instrument responses, we performed data fittings for the selection of time domain (TD) waveforms and cross-correlation (CC) functions. This combination provided the most stable moment tensor results. Previous publications (e.g., Cabieces et al., 2020; Kühn et al., 2020) indicate that, especially in case of unreliable waveform information, cross-correlation functions can be used to improve depth and location estimates and employ phase information that otherwise would be lost. Figure 37 illustrates the stations of which transverse (Figure 37a), radial (Figure 37c) and vertical (Figure 37e) components were chosen for data fitting in time domain based on SNR. The significant part of the stations showing large discrepancies between observed and synthetic traces was only used for cross-correlation data fitting: Figure 37b displays stations of which transverse, Figure 37d stations of which radial and Figure 37f stations of which vertical components were employed. Figure 38 shows examples of waveforms fitting (a) in time and (b) in cross-correlation domain for a selection of stations.

5.5 Results

After computations are finalised, Grond creates an HTML report for the earthquake source inversion results, which include the best (Table 1) and mean parameter results, waveform fit plots for the best model (examples in Figure 38), histogram plots of the inverted parameters (Figures 41 and 42), the distribution of location estimates (Figure 39), a moment tensor decomposition (Figure 40), a Hudson plot (Figure 43) and others. The best solution agrees with the mean solution, and the event location is well-confined, which confirms the stability of the acquired result.

The resulting solution for the 21st of March 2022 event is similar to previously published results (Zarifi et al., 2022; Jerkins et al., 2023) and the solution published in the Global Centroid Moment tensor (Global CMT) catalogue by Dziewonski et al. (1981a) (see Figure 44). The results of these independent studies, with different input data, velocity models have a good agreement with each other. The differences can be observed in the depth estimations. Depth estimation of the current studies lies between the values acquired by Zarifi et al. (2022) and Jerkins et al. (2023). Jerkins et al. (2023) conducted a grid search for the hypocentral depth and obtained the estimation of 14.4±3.7 km. Zarifi et al. (2022) reported the depth estimation of 17 km. Significant north and east shifts of the centroid location can be explained by the inaccurate initial location reported by the ISC (International Seismological Centre, 2022). The reported source location in the bulletin is ≈20km away from the calculated mainshock coordinates by Jerkins et al. (2023). In addition, the centroid moment tensor provides an estimation of the source centroid, which represents the spatial and temporal centre of the moment of the earthquake, which, especially for larger earthquakes, can differ from the hypocenter location. Furthermore, the observed shifts are in the order of the error estimations described in the section 2.2 on event relocations.

Similar parameters as derived from the earthquake of the 21st of March 2022 were employed to invert data from the 9th of October 2016 (12:48:30 GMT) and the 24th of September 2019 (13:38:14 GMT) events. The focal mechanism for the 24th of September 2019 (13:38:14 GMT) complies with the

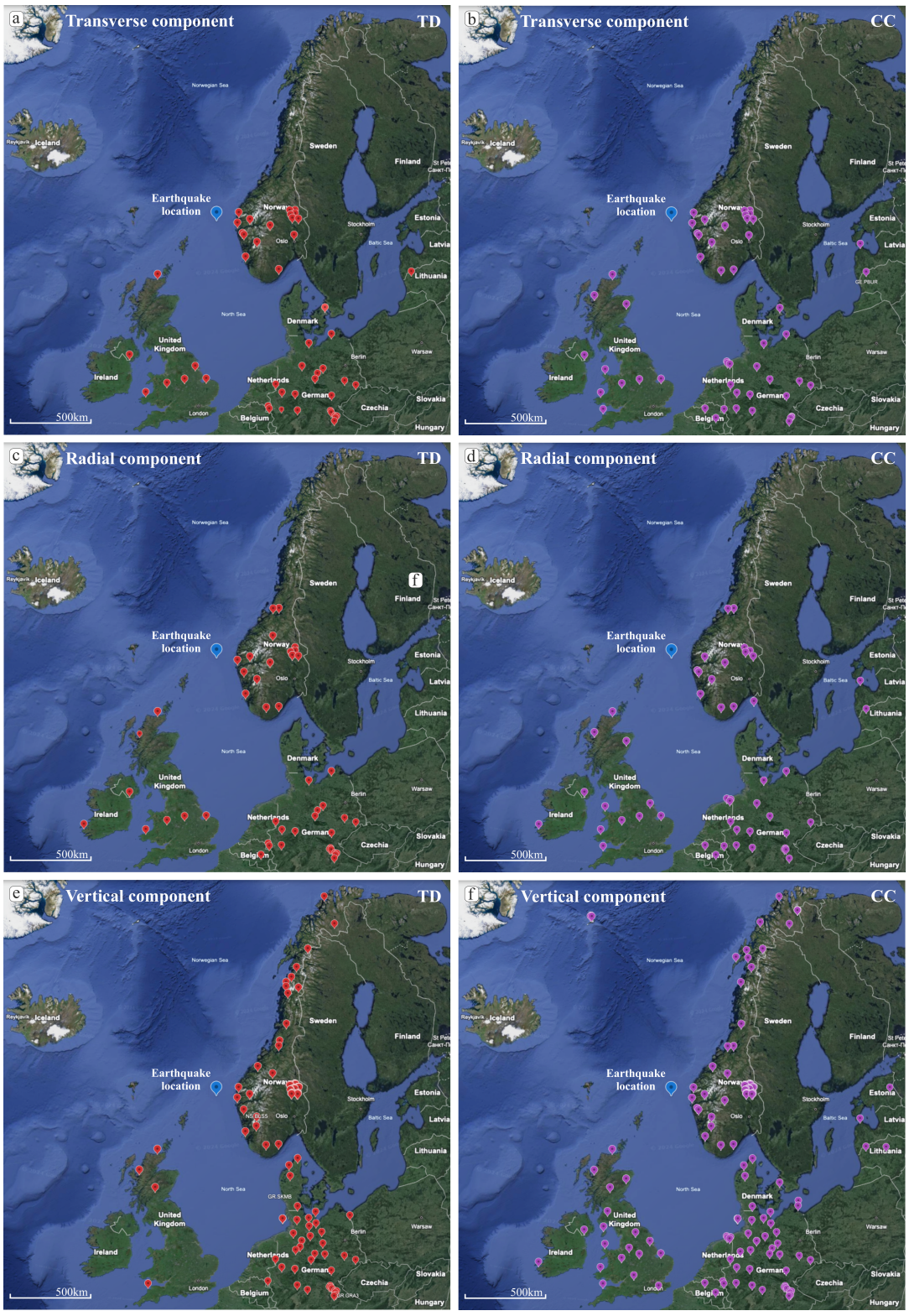

FIGURE 37: The locations of the stations selected for the moment tensor inversion in time domain (TD) (a) transverse, (c) radial, (e) vertical components as well as in cross-correlation domain (CC) (b) transverse, (d) radial, (f) vertical components.

previously published solution by the International Seismological Centre (2022) (Figure 45). The newly acquired solution has a depth of 3.4 km. The ISC catalogue has a depth value of 10 km, which, most likely, was inserted as the standard value in case of the absence of depth estimations calculated for

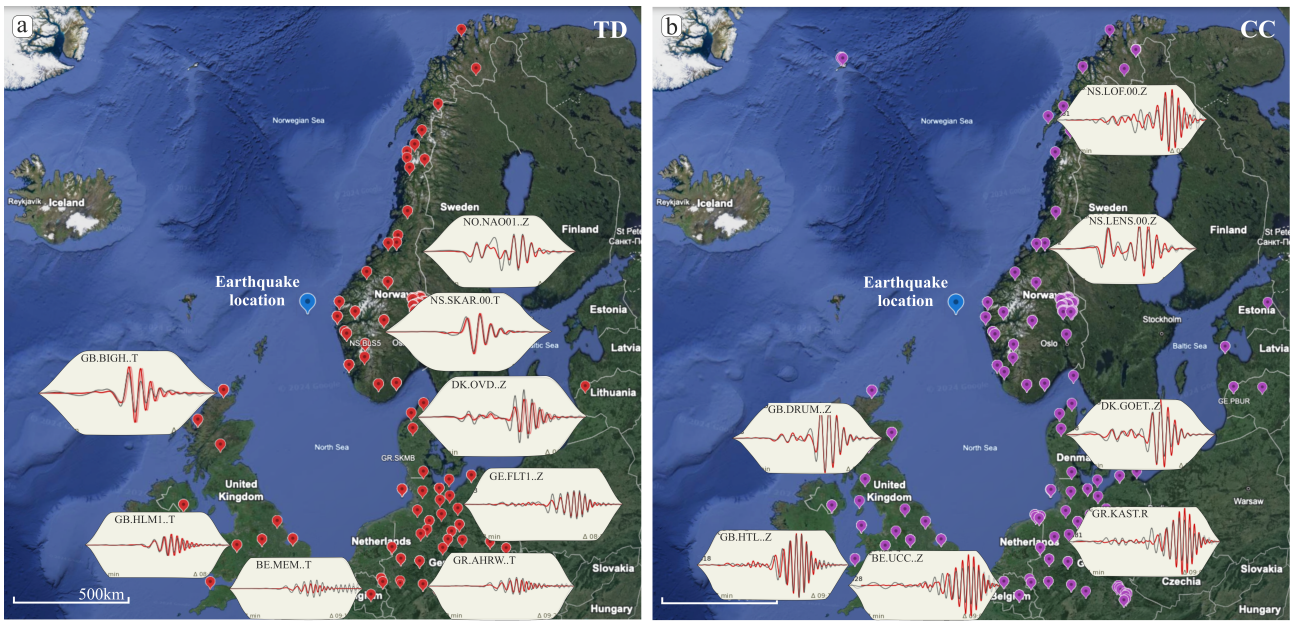

FIGURE 38: The location of the stations selected for the moment tensor inversion with examples of waveforms fits (a) in time and (b) cross-correlation domain.

this event.

The solution for the earthquake that occurred on the 9th of October 2016 (12:48:30 GMT), also has a good agreement with the solution published by the GCMT and GEOFON (Figure 46). In the GCMT catalogue, the reported depth is 27 km, and GEOFON states 10 km depth, which most likely corresponds to a standard value used in case no depth estimation was provided. Our solution has a depth estimation of 14.3 km. The confidence interval for the depth estimation is relatively narrow (see Figure 47a); therefore, we are confident in the provided evaluation. However, more investigation is needed to understand the possible reasons for the significant differences in depth values provided by different catalogues.

Figure 47 shows histograms for the depth estimation of the three focal mechanisms discussed before. In the case of the 21st of March 2022, the 90% confidence interval is the most narrow, which hints toward reliable moment tensor parameters provided by the inversion. Depth calculated for the 24th of September 2019 (13:38:14 GMT) event has wider 90% confidence interval, but still relatively well confined. The assessment for the the 9th of October 2016 (12:48:30 GMT) has a relatively narrow 90% confidence interval, similar to the 21st of March 2022 event. These newly computed solutions for the North Sea region are plotted in Figure 48 in light blue color. The newly computed magnitudes are classified as moment centroid Mwc (see Table 2) since they were derived from a centroid moment tensor inversion of the long-period surface waves (United States Geological Survey, 2022). Table 2 shows a comparison between the Mwc and moment magnitudes (Mw) listed in the bulletin. The observed difference between Mwc's and Mw's values is in the range of 0.01-0.2 and indicates good agreement between these two estimations. However, more Mwc's values are required for a more sophisticated analysis.

Computations for a further five events are ongoing but are hindered by the significant azimuthal gap

caused by the absence of stations toward the north, even for the most recent events, quite often exceeding 180°. An additional complication is related to the signal-to-noise ratio variation throughout the dataset. All these factors limit the stability of the moment tensor inversion. A preliminary unvalidated solutions for the 16th of August 2012 (20:30:33 GMT), the 16th of October 2014 (22:43:45 GMT) and the 30th of June 2017 (13:33:52 GMT) are plotted in Figure 48 in orange.

The non-double-couple (NDC) components of the newly computed solutions can be explained by various reasons, such as source complexity and complexity of the source-receiver paths, which may not be adequately captured by the 1D layered model, or they could be artefacts of the moment tensor inversion process (Rösler et al., 2024). One of the most recent studies suggests that NDC components for individual earthquakes with Mw<6.5 are only weakly correlated between different catalogues (Rösler et al., 2024).

Other events, such as the earthquakes that occurred on the 22nd of February 2020 (18:42:56 GMT), the 25th of March 2022 (04:56:37 GMT), the 16th of September 2018 (08:57:42 GMT), the 9th of June 2018 (22:14:25 GMT), the 7th of November 2017 (08:46:34 GMT), the tth of July 2017 (01:42:42 GMT), the 9th of September 2016 (22:00:42 GMT), the 11th of December 2015 (07:20:45 GMT), the 6th of August 2015 (15:03:59 GMT), the 16th of April 2011 (08:29:06 GMT), and the 16th of February 2011 (04:30:15 GMT) do not have sufficient data for the computations.

TABLE 1: Best moment tensor solution for the 21st of March 2022 event

Parameter	Value
Latitude	61.53°
Longitude	2.53°
North shift	36.58 km
East shift	-23.96 km
Time	2022-03-21 05:32:56.57
Depth	15.56 km
Magnitude	5.15
Moment tensor	
Strike	161.00°
Dip	44.13°
Rake	65.22°

TABLE 2: The comparison of the moment magnitudes calculated using Grond algorithm for moment tensor inversion and reported in the seimological bulletin.

Event	Mwc	Mw catalogue	Reported by
10/09/2016	4.35	4.4 / 4.8	GEOFON / GCMT
24/09/2019	3.9	4.10	Kiel
21/03/2021	5.15	5.14	ISC

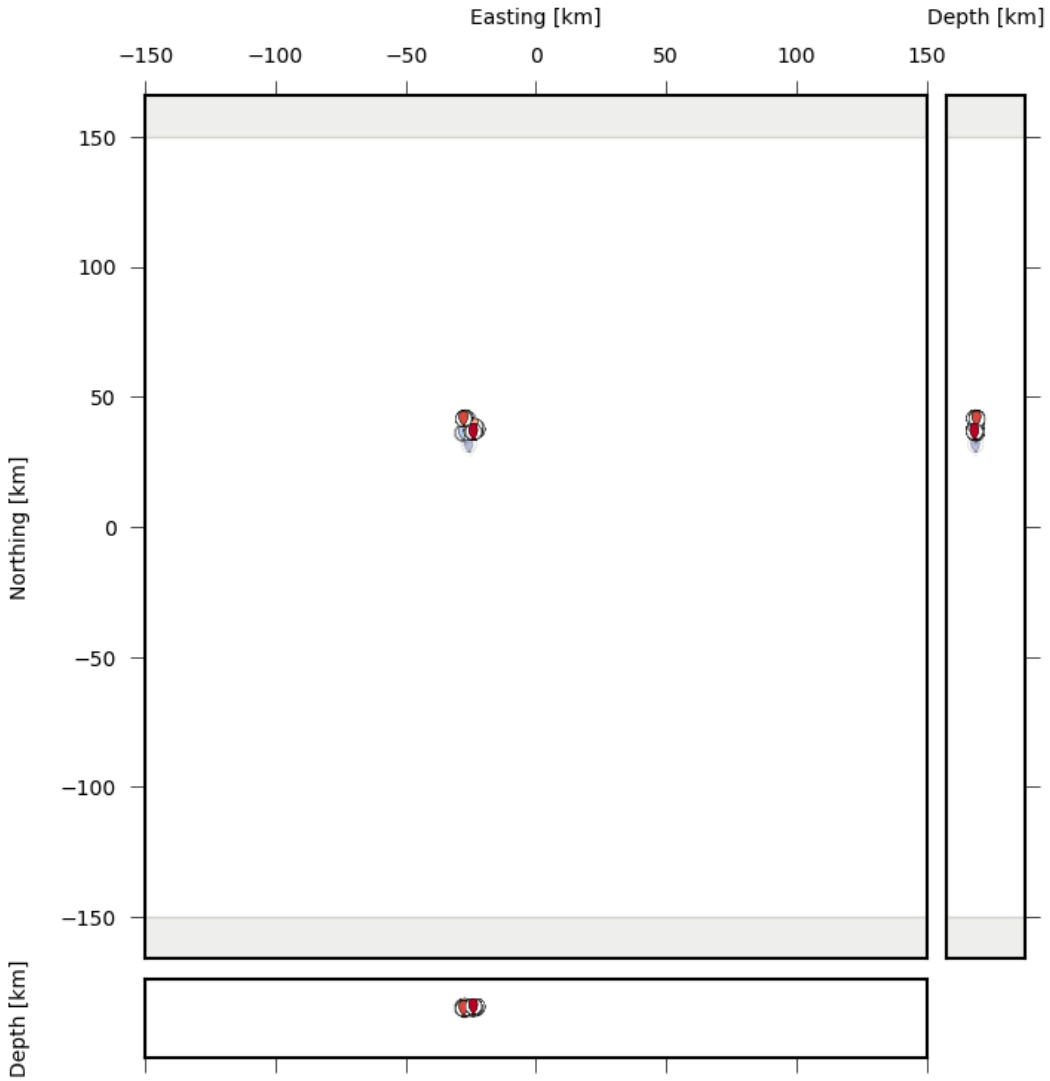

FIGURE 39: Location of the ensemble of 100 best solutions in three cross-sections for the earthquake of 21 March 2022.

5.6 Recommendations

To improve moment tensor inversion using the surface wave time window and suggested methodology:

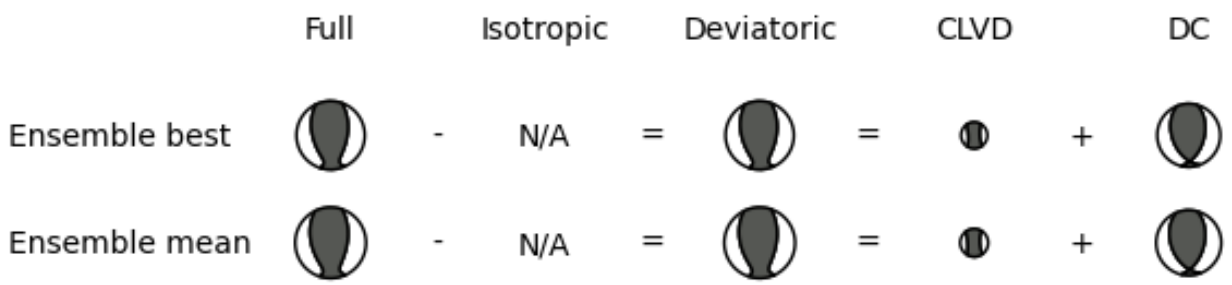

FIGURE 40: Moment tensor decomposition of the best-fitting solution into deviatoric and best double-couple components.

1. Include additional data from seismological networks such as VI (Icelandic National Digital Seismograph Network, which is operated by the Icelandic Meteorological Office). This will allow to reduce the azimuthal gap and improve the stations' coverage.
2. Collection of the additional data from the FR (RESIF and other broad-band and accelerometric permanent networks in metropolitan France), HE (Finnish National Seismic Network), and FN (Northern Finland Seismological Network) could make the inversion more stable for the large magnitude events.
3. Install offshore stations for permanent monitoring to reduce the azimuthal gap and improve the station coverage, with the goal of increasing the number of near-source observations. Tiira et al. (2016) show that to resolve events with the magnitude 0, the azimuthal gap needs to be smaller than 180°.
4. Start using dense networks utilising fibre optics. However, this requires knowledge of the instrument response of fibre optic cables to enable the representation of true ground motion amplitudes.
5. Improve the knowledge on station installation conditions (soft/hard ground) to understand which type of amplitude corrections to include.
6. Create a reasonably accurate regional velocity model of the North Sea. With a more detailed velocity model, waveform fits can be improved, especially at higher frequencies, which will be crucial for the focal mechanisms inversions of the small magnitude events.
7. Improve the knowledge of the attenuation models and site amplification.

In addition to the suggested approach, computing moment tensor using surface waves and extensive testing using other wave types will be beneficial.

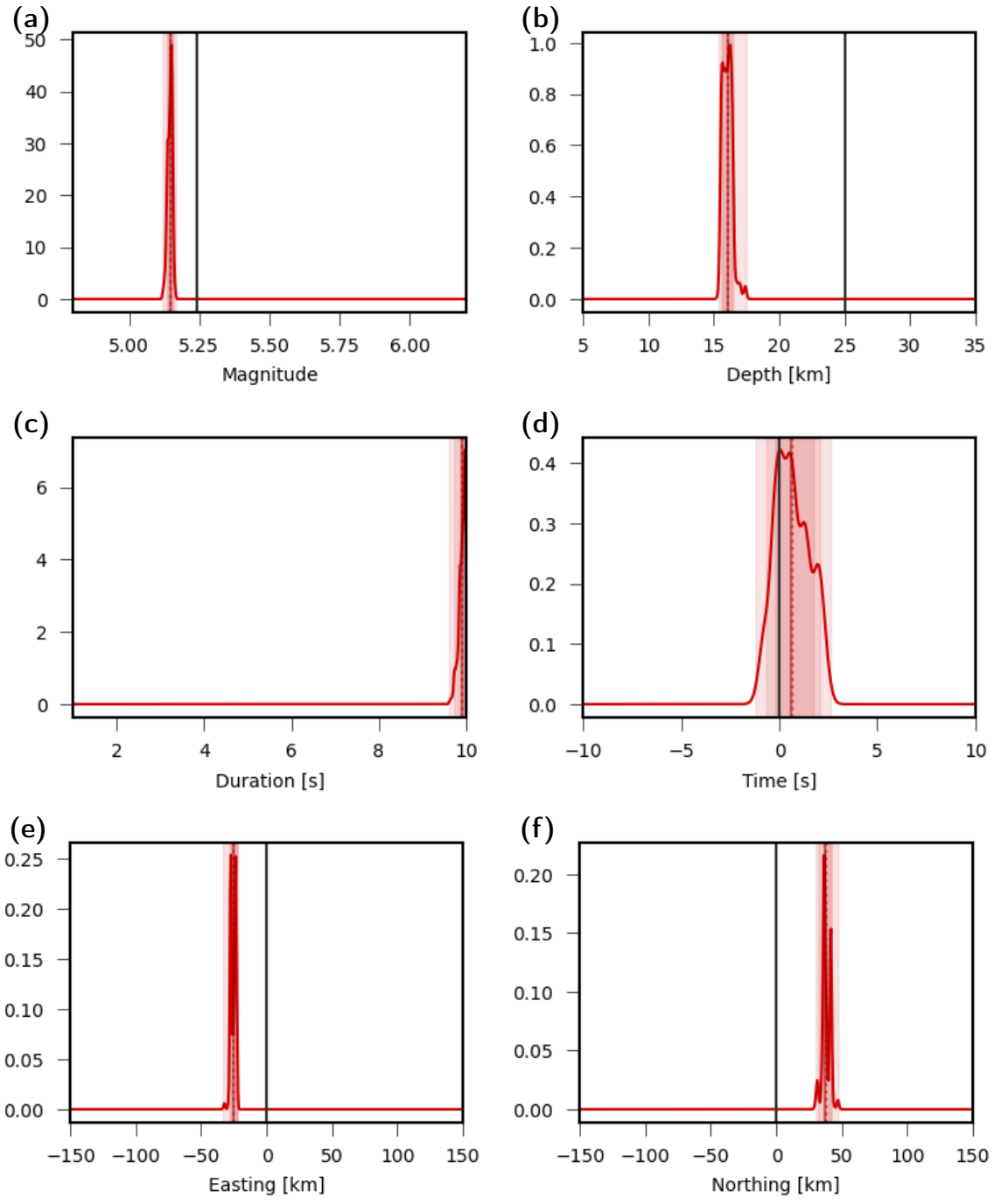

FIGURE 41: Distribution of the inverted parameters: (a) magnitude, (b) depth [km], (c) duration [s], (d) origin time [s], (e) easting [km] and northing [km]. The overlapping red-shaded areas show the 68% confidence intervals (innermost area), the 90% confidence intervals (middle area) and the minimum and maximum values (widest area). The plot ranges are defined by the given parameter bounds and illustrate the model space.

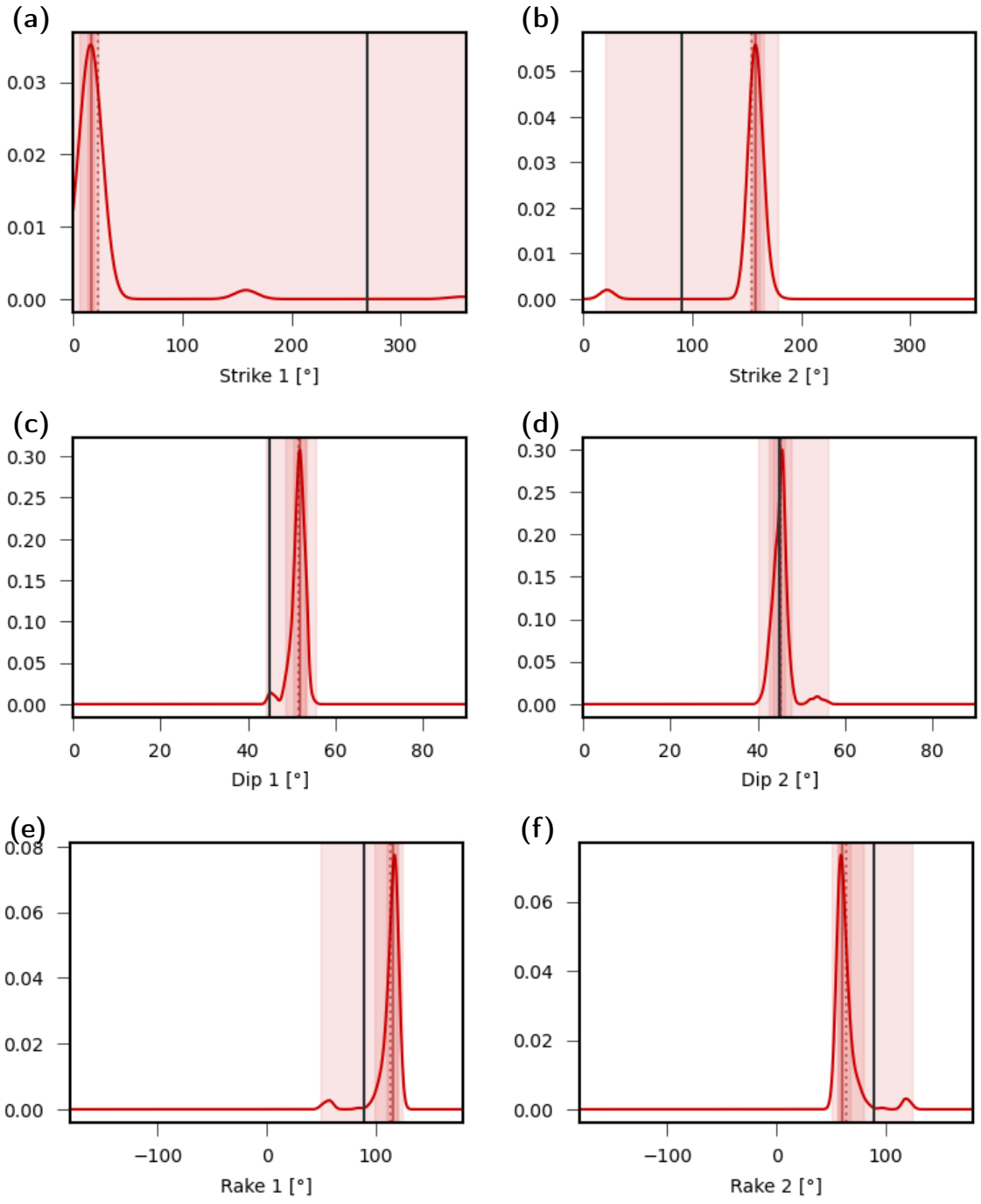

FIGURE 42: Distribution of the inverted parameters: (a) strike 1 [°], (b) strike 2 [°], (c) dip 1 [°], (d) dip 2 [°], (e) rake 1 [°] and rake 2 [°]. The overlapping red-shaded areas show the 68% confidence intervals (innermost area), the 90% confidence intervals (middle area) and the minimum and maximum values (widest area). The plot ranges are defined by the given parameter bounds and illustrate the model space.

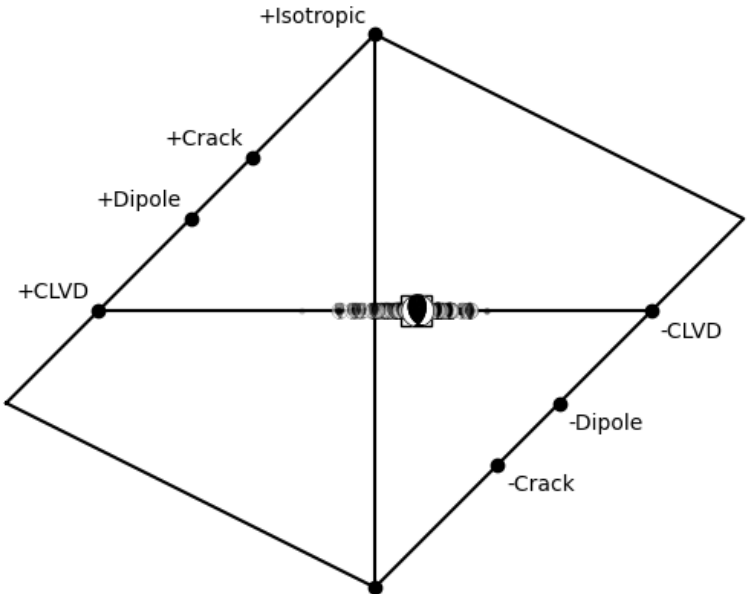

FIGURE 43: Hudson plot displaying the decomposition of moment tensor components into their isotropic (ISO), double-couple (DC), compensated linear vector dipole (CLVD) parts (see Hudson et al., 1989) with the ensemble of bootstrap solutions. The best solution is identified by a square, the mean by a large beachball. The deviatoric solution excludes the computation of isotropic components, and therefore, the estimated moment tensor solutions align on the CLVD axis.

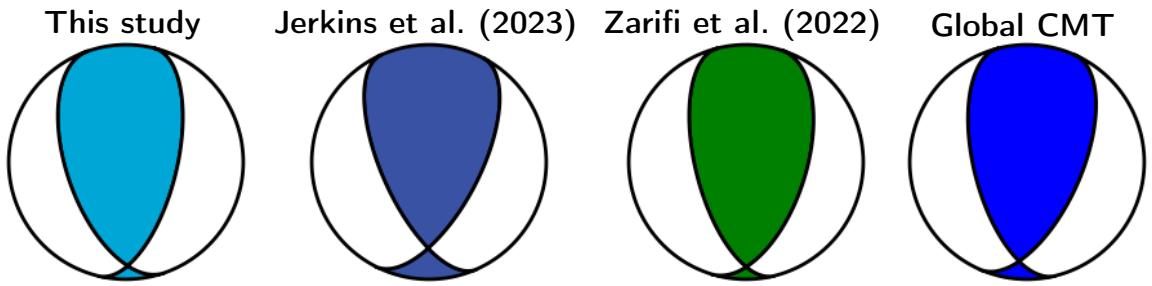

FIGURE 44: A comparison of the existing moment tensor solution for the 21st of March 2022: (a) this study, (b) Jerkins et al. (2023), (c) Zarifi et al. (2022) and (d) Global Centroit Moment tensor (Global CMT) catalogue. The parameters of the nodal plane (NP) 1 and 2 are given by the strike, dip, and rake, respectively, as well as the best-fitting depth below each moment tensor solution.

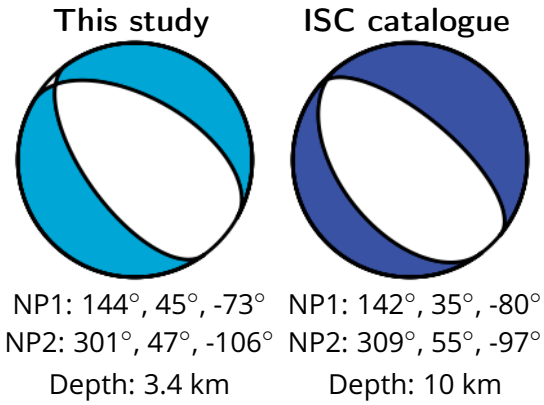

FIGURE 45: A comparison of the existing moment tensor solution for the 24st of September 2019: (a) this study, (b) the ISC catalogue. The parameters of the nodal plane (NP) 1 and 2 are given by the strike, dip, and rake, respectively, as well as the best-fitting depth below each moment tensor solution.

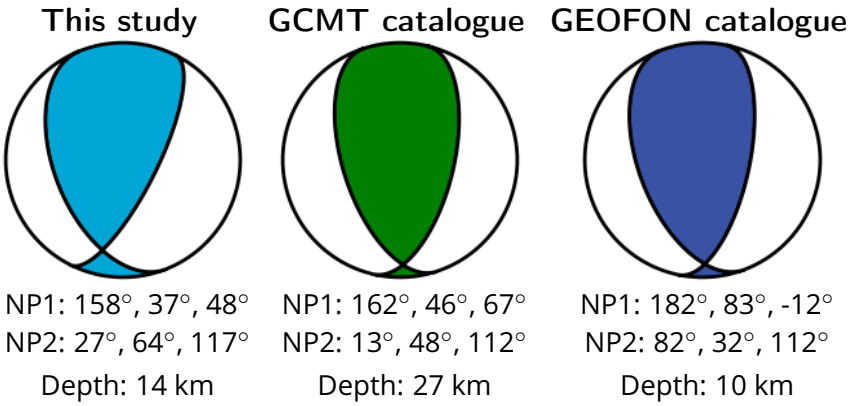

FIGURE 46: A comparison of the existing moment tensor solution for the 9th of October 2016: (a) this study, (b) the GCMT and GEOFON catalogues. The parameters of the nodal plane (NP) 1 and 2 are given by the strike, dip, and rake, respectively, as well as the best-fitting depth below each moment tensor solution.

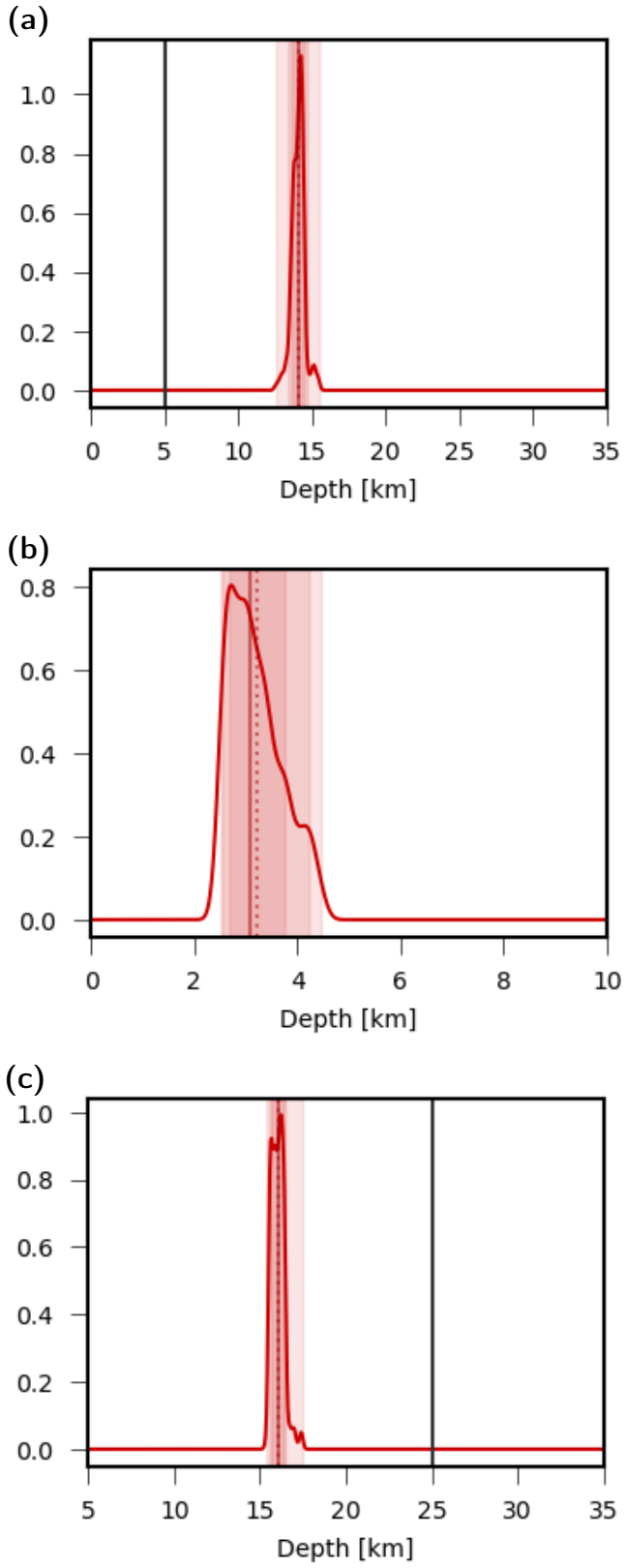

FIGURE 47: A comparison of the uncertainties for the depth estimations for the newly computed focal mechanisms: (a) the 9th of October 2016, (b) the 24st of September 2019, (c) the 21st of March 2022. The overlapping red-shaded areas show the 68% confidence intervals (inner-most area), the 90% confidence intervals (middle area) and the minimum and maximum values (widest area). The plot ranges are defined by the given parameter bounds and illustrate the model space.

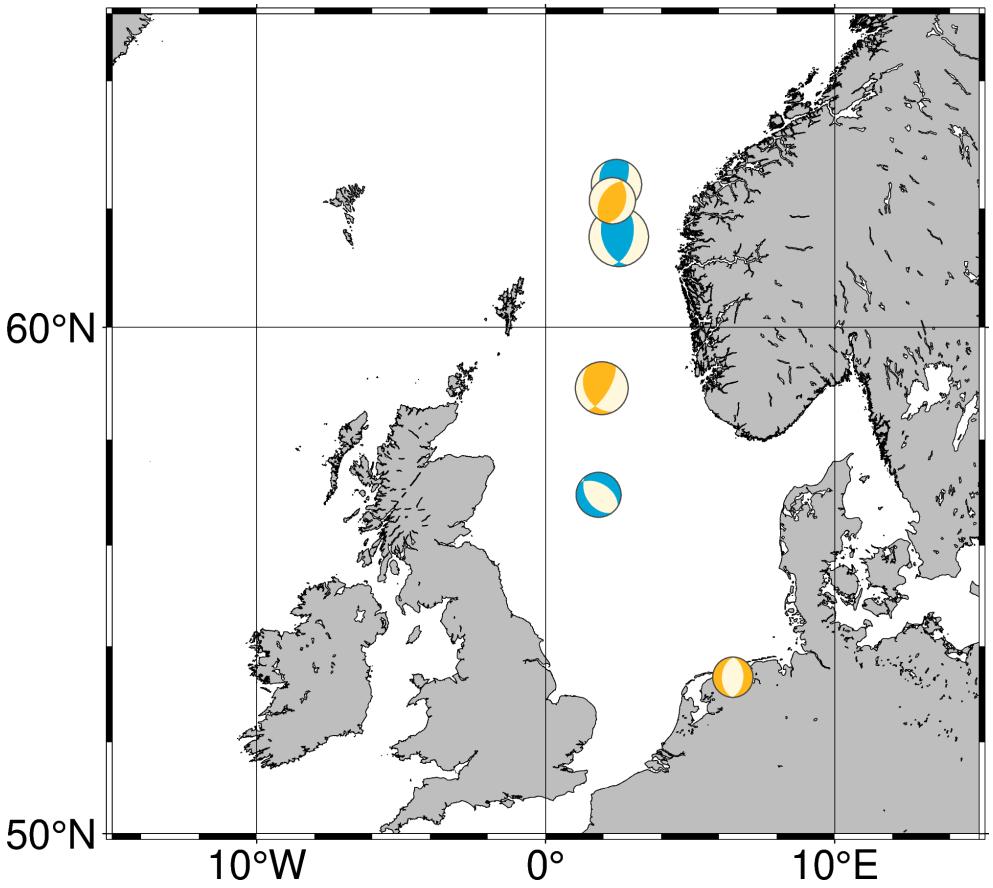

FIGURE 48: Map of the computed moment tensors in the North Sea region. The moment tensor solutions shown in orange are preliminary results and are still to be validated and finalised.

References

Beyreuther, M., R. Barsch, L. Krischer, T. Megies, Y. Behr, and J. Wassermann (2010). "ObsPy: A Python toolbox for seismology". In: *Seismological Research Letters* 81.3, pp. 530–533.

Bondár, I. and D. Storchak (2011). "Improved location procedures at the International Seismological Centre". In: *Geophysical Journal International* 186.3, pp. 1220–1244.

British Geological Survey (1970). *Great Britain Seismograph Network*. DOI: 10.7914/AV8J-NC83. URL: https://www.fdsn.org/networks/detail/GB/.

Cabieces, Roberto, Elisa Buforn, Simone Cesca, and Antonio Pazos (Apr. 2020). "Focal Parameters of Earthquakes Offshore Cape St. Vincent Using an Amphibious Network". In: *Pure and Applied Geophysics* 177. DOI: 10.1007/s00024-020-02475-3.

Christian Albrechts - Universitat zu Kiel (2017). *Kiel University Earthquake Monitoring*. DOI: 10.7914/SN/KQ. URL: https://www.fdsn.org/networks/detail/KQ/.

Dost, Bernard, Benjamin Edwards, and Julian J. Bommer (May 2018). "The Relationship between M and ML: A Review and Application to Induced Seismicity in the Groningen Gas Field, The Netherlands". In: *Seismological Research Letters* 89 (3), pp. 1062–1074. ISSN: 0895-0695. DOI: 10.1785/0220170247. URL: https://pubs.geoscienceworld.org/ssa/srl/article/89/3/1062/529916/The-Relationship-between-M-and-ML-A-Review-and.

Dziewonski, A. M., T.-A. Chou, and J. H. Woodhouse (1981a). "Determination of earthquake source parameters from waveform data for studies of global and regional seismicity". In: *Journal of Geophysical Research: Solid Earth* 86.B4, pp. 2825–2852. DOI: https://doi.org/10.1029/JB086iB04p02825. eprint: https://agupubs.onlinelibrary.wiley.com/doi/pdf/10.1029/JB086iB04p02825. URL: https://agupubs.onlinelibrary.wiley.com/doi/abs/10.1029/JB086iB04p02825.

Dziewonski, Adam M, T-A Chou, and John H Woodhouse (1981b). "Determination of earthquake source parameters from waveform data for studies of global and regional seismicity". In: *Journal of Geophysical Research: Solid Earth* 86.B4, pp. 2825–2852.

Ekström, Göran, Meredith Nettles, and AM Dziewoński (2012). "The global CMT project 2004–2010: centroid-moment tensors for 13,017 earthquakes". In: *Physics of the Earth and Planetary Interiors* 200, pp. 1–9.

Federal Institute for Geosciences and Natural Resources (1976). *German Regional Seismic Network (GRSN)*. https://doi.org/10.25928/mbx6-hr74. Seismic Network.

German Research Centre for Geosciences GFZ (1993). *GEOFON Seismic Network [Data set]*. Seismic Network. URL: https://doi.org/10.14470/TR560404.

Gibbons, S.J., G. Antonovskaya, V. Asming, Y.V. Konechnaya, E. Kremenetskaya, T. Kværna, J. Schweitzer, and N.V. Vaganova (June 2016). "The 11 October 2010 Novaya Zemlya earthquake: implications for velocity models and regional event location". In: *Bulletin of the Seismological Society of America* 106.4, pp. 1470–1481. ISSN: 0037-1106. DOI: 10.1785/0120150302. eprint: https://pubs.geoscienceworld.org/ssa/bssa/article-pdf/106/4/1470/2645467/1470.pdf. URL: https://doi.org/10.1785/0120150302.

Gregersen, Søsren and Franco Vaccari (July 1993). "Lg-Wave Modelling For the North Sea". In: *Geophysical Journal International* 114 (1), pp. 76–80. ISSN: 0956540X. DOI: 10.1111/j.1365-246X.1993.tb

01467.x. URL: https://academic.oup.com/gji/article-lookup/doi/10.1111/j.1365-246X.1993.tb01467.x.

Havskov, J., P. Bormann, and J. Schweitzer (2012). "Seismic source location". In: *New Manual of Seismological Observatory Practice 2 (NMSOP-2)*. Deutsches GeoForschungsZentrum GFZ, pp. 1–36.

Heimann, S. et al. (2017). *Pyrocko - an open-source seismology toolbox and library*. GFZ Data Services.

Heimann, Sebastian, Marius Isken, Daniela Kühn, Henriette Sudhaus, Andreas Steinberg, Hannes Vasyura-Bathke, Simon Daout, Simone Cesca, and Torsten Dahm (2018). *Grond - A probabilistic earthquake source inversion framework*. Version 1.0. DOI: 10.5880/GFZ.2.1.2018.003. URL: http://pyrocko.org/grond/docs/current/ (visited on 08/27/2018).

Helmholtz-Centre Potsdam - GFZ German Research Centre for Geosciences and gempa GmbH (2008). *The SeisComP seismological software package. GFZ Data Services.* DOI: 10.5880/GFZ.2.4.2020.003. URL: https://www.seiscomp.de.

Hicks, E.C., T. Kværna, S. Mykkeltveit, J. Schweitzer, and F. Ringdal (2004). "Travel-times and attenuation relations for regional phases in the Barents Sea region". In: *Pure and Applied Geophysics* 161, pp. 1–19.

Hudson, J. A., R. G. Pearce, and R. M. Rogers (1989). "Source type plot for inversion of the moment tensor". In: *Journal of Geophysical Research: Solid Earth* 94.B1, pp. 765–774. DOI: https://doi.org/10.1029/JB094iB01p00765. eprint: https://agupubs.onlinelibrary.wiley.com/doi/pdf/10.1029/JB094iB01p00765. URL: https://agupubs.onlinelibrary.wiley.com/doi/abs/10.1029/JB094iB01p00765.

International Seismological Centre (2022). *Online bulletin*. http://www.isc.ac.uk/iscbulletin/search/.

Jerkins, Annie E., Volker Oye, Celso Alvizuri, Felix Halpaap, and Tormod Kværna (Nov. 2023). "The 21 March 2022 Mw 5.1 Tampen Spur Earthquake, North Sea: Location, Moment Tensor, and Context". In: *Bulletin of the Seismological Society of America* 114.2, pp. 741–757. ISSN: 0037-1106. DOI: 10.1785/0120230163. eprint: https://pubs.geoscienceworld.org/ssa/bssa/article-pdf/114/2/741/6338937/bssa-2023163.1.pdf. URL: https://doi.org/10.1785/0120230163.

Kühn, Daniela, Sebastian Heimann, Marius P Isken, Elmer Ruigrok, and Bernard Dost (2020). "Probabilistic moment tensor inversion for hydrocarbon-induced seismicity in the Groningen gas field, The Netherlands, Part 1: Testing". In: *Bulletin of the Seismological Society of America* 110.5, pp. 2095–2111.

Laske, G., G. Masters, Z. Ma, and M. Pasyanos (2013). "Update on CRUST1.0 — A 1-degree global model of Earth's crust". In: *Geophysical Research Abstracts*. Vol. 15. EGU General Assembly Vienna, Austria, p. 2658.

Lentas, K (2018). "Towards routine determination of focal mechanisms obtained from first motion P-wave arrivals". In: *Geophysical Journal International* 212.3, pp. 1665–1686.

Lentas, Konstantinos, Domenico Di Giacomo, James Harris, and Dmitry A Storchak (2019). "The ISC Bulletin as a comprehensive source of earthquake source mechanisms". In: *Earth System Science Data* 11.2, pp. 565–578.

Luckett, Richard, Lars Ottemöller, Antony Butcher, and Brian Baptie (2019). "Extending local magnitude ML to short distances". In: *Geophysical Journal International* 216 (2), pp. 1145–1156. ISSN: 1365246X. DOI: 10.1093/gji/ggy484.

Menke, W. (2018). *Geophysical Data Analysis: Discrete inverse theory*. Academic press.

Mykkeltveit, S. and F. Ringdal (1981). "Phase identification and event location at regional distance using small-aperture array data". In: *Identification of Seismic Sources—Earthquake or Underground Explosion: Proceedings of the NATO Advance Study Institute held at Voksenåsen, Oslo, Norway, September 8–18, 1980*. Springer, pp. 467–481.

NORSAR (1971). *NORSAR Station Network [Data set]*. https://doi.org/10.21348/d.no.0001. Seismic Network.

Petersen, G. M., S. Cesca, S. Heimann, P. Niemz, T. Dahm, D. Kühn, J. Kummerow, T. Plenefisch, the AlpArray, and AlpArray-Swath-D working groups (2021). "Regional centroid moment tensor inversion of small to moderate earthquakes in the Alps using the dense AlpArray seismic network: challenges and seismotectonic insights". In: *Solid Earth* 12.6, pp. 1233–1257. DOI: 10.5194/se-12-1233-2021. URL: https://se.copernicus.org/articles/12/1233/2021/.

Quinteros, Javier, Angelo Strollo, Peter L Evans, Winfried Hanka, Andres Heinloo, Susanne Hemmleb, Laura Hillmann, Karl-Heinz Jaeckel, Rainer Kind, Joachim Saul, et al. (2021). "The GEOFON program in 2020". In: *Seismological Research Letters* 92.3, pp. 1610–1622.

Rösler, Boris, Seth Stein, Adam Ringler, and Jiří Vackář (2024). "Apparent Non-Double-Couple Components as Artifacts of Moment Tensor Inversion". In: *Seismica* 3.1. DOI: 10.26443/seismica.v3i1.1157. URL: https://seismica.library.mcgill.ca/article/view/1157.

Royal Netherlands Meteorological Institute (KNMI) (1993). *Netherlands Seismic and Acoustic Network*. https://doi.org/10.21944/e970fd34-23b9-3411-b366-e4f72877d2c5. Seismic Network.

Royal Observatory of Belgium (1985). *Belgian Seismic Network [Data set]*. https://doi.org/10.7914/SN/BE. Seismic Network.

Schweitzer, J. (2001). "HYPOSAT - an enhanced routine to locate seismic events". In: *Pure and Applied Geophysics* 158, pp. 277–289.

Schweitzer, J. and B.L.N. Kennett (2007). "Comparison of location procedures: the Kara Sea event of 16 August 1997". In: *Bulletin of the Seismological Society of America* 97.2, pp. 389–400.

Schweitzer, J., B. Paulsen, G.N. Antonovskaya, A.V. Fedorov, Y.V. Konechnaya, V.E. Asming, and M. Pirli (2021). "A 24-yr-long seismic bulletin for the European Arctic". In: *Seismological Research Letters* 92.5, pp. 2758–2767.

Seismisk Tjeneste (2023). *National Seismic Network for the Kingdom of Denmark*. http://seis.geus.net/. Geological Survey of Denmark and Greenland, Copenhagen, Denmark.

Shearer, Peter M. (2019). *Introduction to Seismology*. 3rd ed. Cambridge University Press. Chap. 9.

Sollberger, David (July 2023). *solldavid/TwistPy: TwistPy - First release*. Version v0.0.1-beta. DOI: 10.5281/zenodo.8124030. URL: https://doi.org/10.5281/zenodo.8124030.

Stange, S. and J. Schweitzer (2004). "Source depths at regional distances: an example from the western Barents Sea/Svalbard region". In: *NORSAR Scientific Report* 1.2004, pp. 45–50.

Stork, A.L., J.P. Verdon, and J.-M. Kendall (July 2014). "The robustness of seismic moment and magnitudes estimated using spectral analysis". In: *Geophysical Prospecting* 62 (4), pp. 862–878. ISSN:

0016-8025. DOI: 10.1111/1365-2478.12134. URL: https://onlinelibrary.wiley.com/doi/10.1111/1365-2478.12134.

Tiira, Timo, Marja Uski, J. Kortström, Outi Kaisko, and A. Korja (Apr. 2016). "Local seismic network for monitoring of a potential nuclear power plant area". In: *Journal of Seismology* 20. DOI: 10.1007/s10950-015-9534-8.

Tjåland, N (2020). *Determination of fault plane solutions using P-wave polarities*. Tech. rep. NNSN, University of Bergen.

Tjåland, N and L Ottemöller (2018). *Evaluation of seismicity in the Northern North Sea*. Tech. rep. NNSN, University of Bergen.

United States Geological Survey (2022). *Magnitude Types*. https://www.usgs.gov/programs/earthquake-hazards/magnitude-types.

University of Bergen (1982). *University of Bergen Seismic Network [Data set]*. https://doi.org/10.7914/SN/NS. Seismic Network.

Wang, Rongjiang (June 1999). "A simple orthonormalization method for stable and efficient computation of Green's functions". In: *Bulletin of the Seismological Society of America* 89.3, pp. 733–741. ISSN: 0037-1106. DOI: 10.1785/BSSA0890030733. eprint: https://pubs.geoscienceworld.org/ssa/bssa/article-pdf/89/3/733/5733743/bssa0890030733.pdf. URL: https://doi.org/10.1785/BSSA0890030733.

Weidle, C., V. Maupin, J. Ritter, T. Kværna, J. Schweitzer, N. Balling, H. Thybo, J. I. Faleide, and F. Wenzel (Jan. 2010). "MAGNUS—A seismological broadband experiment to resolve crustal and upper mantle structure beneath the Southern Scandes mountains in Norway". In: *Seismological Research Letters* 81.1, pp. 76–84. ISSN: 0895-0695. DOI: 10.1785/gssrl.81.1.76. eprint: https://pubs.geoscienceworld.org/ssa/srl/article-pdf/81/1/76/2761638/076.pdf. URL: https://doi.org/10.1785/gssrl.81.1.76.

Zarifi, Zoya, Andreas Köhler, Philip Ringrose, Lars Ottemoller, Anne-Kari Furre, Fredrik Hansteen, Annie Jerkins, Volker Oye, Roya Niri, and Roger Bakke (Nov. 2022). "Background Seismicity Monitoring to Prepare for Large-Scale CO2 Storage Offshore Norway". In: *Seismological Research Letters* 94. DOI: 10.1785/0220220178.

A Squirrel operating mode

The following description is a shortened quotation from the webpages https://pyrocko.org/docs/current/topics/squirrel.html as well as https://pyrocko.org/docs/current/apps/squirrel/tutorial.html. The Squirrel framework provides a unified interface to query and access seismic waveforms, station metadata and event information from both local file collections and remote data sources. Data is first stored in an internal SQL database, which can handle selections with millions of files and to which data can be added (or from which data can be removed) efficiently at run-time. At the first usage, a new and initially empty Squirrel environment is created on disk consisting of an SQLite database and caches. When files are added to the environment, only a minimal excerpt from the file headers is included in the inventory database including time span, FDSN network/station/location/channel codes and sampling rate. These entities are referred to as "nuts". A nut may represent a station or channel epoch, a snippet of waveform or an instrument response epoch. To enable downloads of waveforms, "waveform promises" need to be created, based on matching channels and time spans, and queried from providers. Thus, data that was missed during a first cycle (e.g. due to connectivity issues) is remembered and can be added during a subsequent cycle. If the promise fails permanently, it is deleted, such that the respective server is not repeatedly queried for non-existent data. In this way, data can be downloaded just when needed and already downloaded data will be used together with local data and metadata through one unified interface. Waveforms are downloaded in chunks of reasonable size, therefore the downloaded time frame may be slightly larger than the requested time span. The downloaded data may be incrementally extended in its time span and only missing blocks will be requested. Squirrel maintains indexes of known files, such that repeated program startups are extremely efficient. Figure 49 sketches the manner in which data is downloaded from a remote FDSN site.

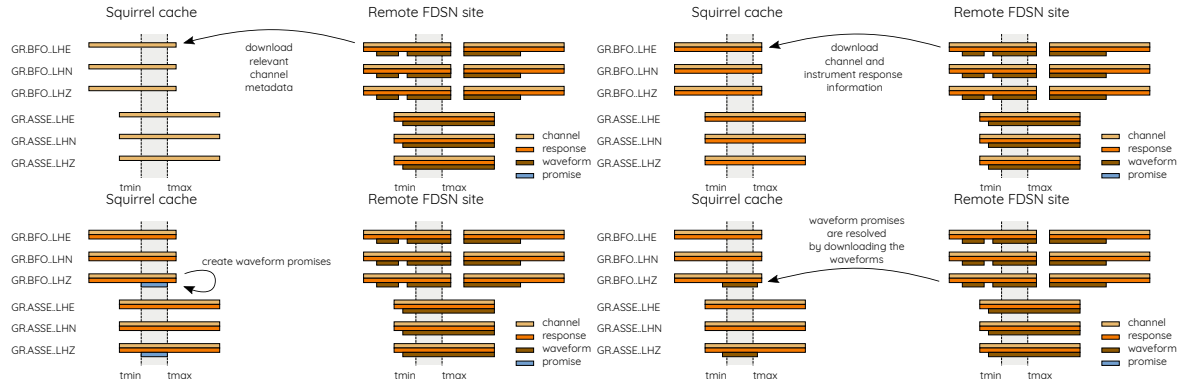

FIGURE 49: Pyrocko (Heimann et al., 2017) Squirrel data download. Upper left: ensuring that the local metadata are up to date by downloading or updating channel epochs intersecting with the defined time span; upper right: optionally, instrument responses may be downloaded for the same time span; lower left: waveform promises are added to selected time intervals on selected channels with the promises acting as placeholders for the waveforms; lower right: matching promises are resolved by downloading the actual waveforms if possible, removing the promises if succeeding. Figures extracted from https://pyrocko.org/docs/current/apps/squirrel/tutorial.html with permission of the authors.

As mentioned above, waveforms are downloaded into a cache directory. They may be transformed subsequently into e.g., a standard SeisComP database with waveform files in MSEED format. In a similar manner, station metadata may be exported to the StationXML format. When adding local data, file formats are autodetected and directories are recursively scanned for any readable files.